IS-T 1872

Liquid Metal Extraction of Nd from NdFeB Magnet Scrap

by

Xu, Yanchen

MS Thesis submitted to Iowa State University

Ames Laboratory, U.S. DOE
Iowa State University
Ames, Iowa 50011

Date Transmitted: December 10, 1999

PREPARED FOR THE U.S. DEPARTMENT OF ENERGY
UNDER CONTRACT NO. W-7405-Eng-82.

DISCLAIMER

DISCLAIMER

Portions of this document may be illegible in electronic image products. Images are produced from the best available original document.

Liquid metal extraction of Nd from NdFeB magnet scrap

Yanchen Xu

Major professor: Scott L. Chumbley

Iowa State University

This research involves using molten magnesium (Mg) to remove neodymium (Nd) from NdFeB magnet scrap by diffusion. Pure Mg was melted over pieces of NdFeB scrap and held at temperatures in the range 675 - 750°C. The Mg was allowed to solidify, and the castings were then sectioned and characterized using scanning electron microscopy (SEM), X-ray diffraction (XRD), and chemical analysis. Nd was found to have diffused rapidly out of the solid scrap into the molten Mg. The thickness of the diffusion layer was measured, the diffusion of Nd through the NdFeB scrap into liquid Mg was described, and the diffusion coefficient of Nd in liquid Mg was estimated. This study shows that liquid metal extraction of Nd may be a viable and inexpensive method for recovering the expensive rare earth element Nd for use in Mg castings.

TABLE OF CONTENTS

1 INTRODUCTION

1.1 General background of NdFeB magnet scrap

Permanent magnets are indispensable components of electromechanical and electronic devices such as computers, printers, motors, microwaves, and audio visual components among others. With the advent of the Sony "Walkman" series of miniaturized portable stereo headphones and tape players, which utilized small but powerful samarium-cobalt magnets, the time of rare-earth-alloy magnet manufacture began. The consumption of samarium oxide in the U. S. was 165th out of all industrial oxides in 1982 despite the fact that its use was totally nonexistent in 1978 [1]. As the demand for permanent rare-earth magnets increased, research was undertaken to develop other rare earth transition-metal compounds that could combine improved magnetic capabilities with lower raw materials costs. The discovery of a stable $Nd_2Fe_{14}B$ phase [2] met the demand for a lower-cost, more readily available material with improved magnet properties.

Ordinary ferrite magnets have a maximum energy product of $36KJ/m^3$; samarium cobalt magnets have maximum energy products over $200KJ/m^3$. NdFeB magnets have the highest energy product of all permanent magnets, over $250KJ/m^3$, and also exhibit excellent resistance to demagnetization at normal operating temperature [3]. NdFeB magnets have become widely used in automotive cranking motors, computers, audio-visual components, magnetic separators, military and aerospace systems, and other devices requiring reduced size and weight [4, 5].

With the expansion of the NdFeB magnet market, the cost and environmental problems associated with their waste and scrap disposal have become an increasing concern.

The high cost of rare earth metals makes simple disposal of rare earth-bearing waste or scrap materials economically unattractive. Up to the present time, there have been no large-scale operations to recover rare earth metals from scrap and waste materials. It is clear that development of a viable method to recycle and reuse NdFeB magnet scrap is desirable for economic and environmental reasons.

There are two major methods, rapid solidification and powder metallurgy techniques, currently being used to manufacture NdFeB magnets. In rapid solidification, a melted alloy is supercooled by generating melt-spun ribbon which is then crushed and treated in further processing steps such as polymer bonding or hot pressing. In this process, material with extremely fine grain size and uniformity of microstructure is obtained which has excellent magnetic properties. Typical scrap types generated by this process are slag and spillage materials from alloy melting, discarded ribbon material, and discarded finished magnets in a variety of forms. Powder metallurgy processing involves the sintering of a powder which is aligned in a magnetic field. This process generates grinding swarf, a mixture of oil, machining chips and other solid residue, in addition to discarded sintered and unsintered (green compact) magnet pieces [6].

The composition of scrap from rapid solidification is similar to that from powder metallurgy processing. All types have the following average composition: 67.3wt.% Fe, 26.3wt.% Nd, 1.85wt.% Pr, and 0.85wt.% B. Because scrap compositions are quite uniform, economical treatment methods were sought which would have the potential to efficiently separate rare-earth metals from iron in all types of NdFeB scrap despite variations in scrap geometry and surface oxidation. A brief summary of several processes along with their advantage and drawbacks is given in the following section.

1.2 Methods currently being investigated

1.2.1 Aqueous based technology

This process begins with the dissolution of the rare earth scrap using HNO_3, H_2SO_4 or HCl in aqueous solution. The insoluble fraction is removed by filtration, and a complete separation of all elements can be accomplished by using solute / solvent extraction or ion exchange technology which are both currently used in producing the rare earth oxides from natural ores. The rare earth elements are then precipitated from solution as an oxalate or a fluoride by the addition of oxalic acid or HF. Selection of a precipitating addition can be made with regard to whether transition metals are to be co-precipitated with the rare earth or not.

During this last decade, the U. S. Department of the Interior Bureau of Mines, investigated several processing techniques for recovery of valuable rare-earth elements from NdFeB magnet scrap. The best separation of rare-earth from the NdFeB magnet scrap was obtained by J.W. Morrison [7], J. W. Lyman [8], and G. R. Palmer using sulfuric acid to dissolve the scrap, followed by precipitation of sodium and ammonium intermediate double salts, i.e. $Nd_2(SO_4)_3 \bullet Na_2SO_4 \bullet 6H_2O$, $NaNd(SO_4)_2 \bullet H_2O$ or $Nd_2(NH_4)_2(SO_4)_4 \bullet 8H_2O$, using an addition of NaOH or NH_4OH. These rare-earth salts were then converted to a variety of useful neodymium products, such as NdF_3 and oxalate by using HF and oxalic acid. The iron-rich effluent following the rare-earth recovery was treated to produce sodium and ammonium iron jarosites ($MFe_3(SO_4)_2(OH)_6$ where M is K^+, Na^+, NH_4^+) that can be disposed of or converted to hematite. Figure 1 is the processing flow sheet illustrating the required stages of aqueous based recycling NdFeB magnet scrap proposed by U. S. Bureau of Mines. In 1993, B. Greenberg [9] obtained neodymium trifluoride from NdFeB swarf, which

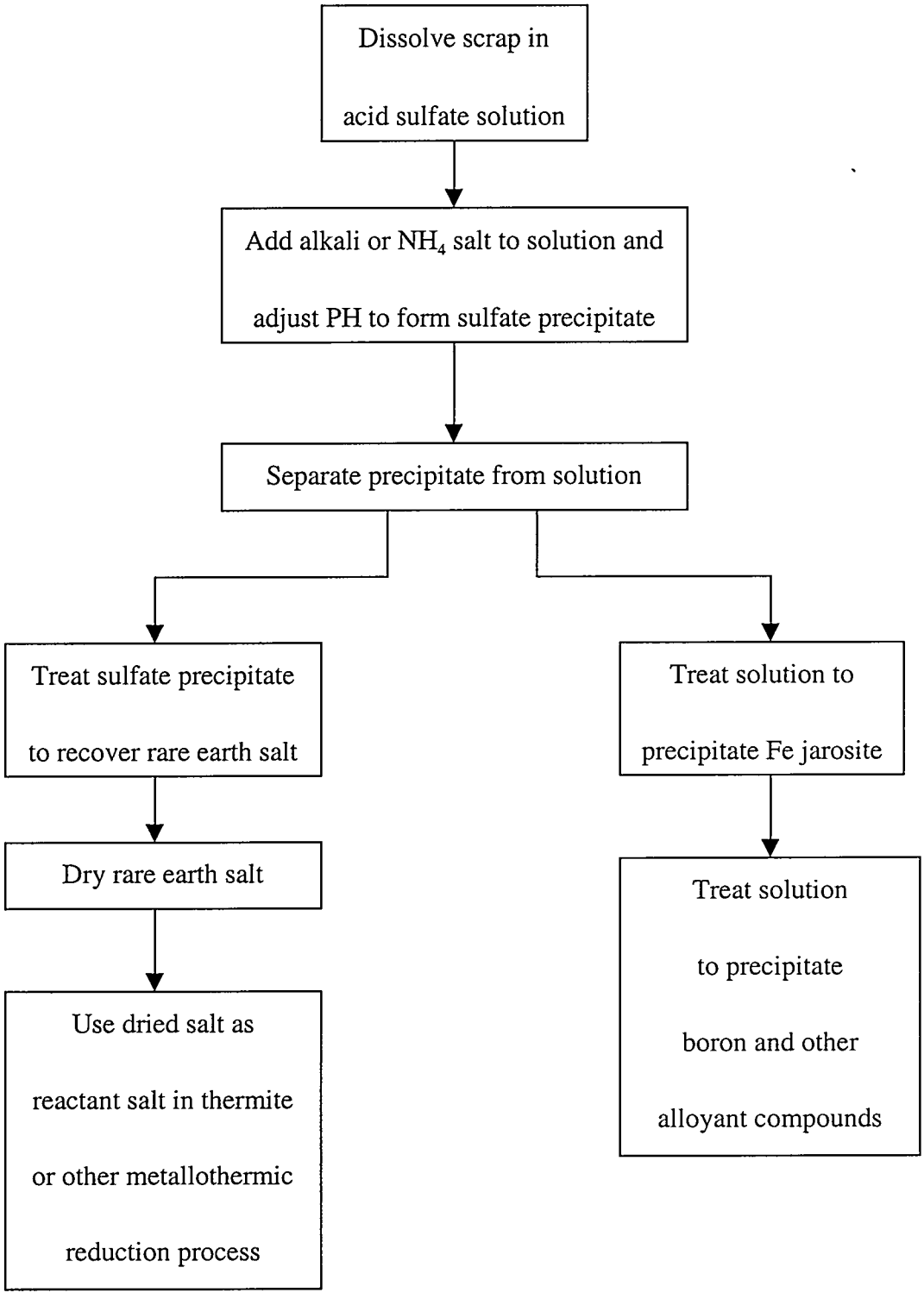

Figure 1. Aqueous based recycling NdFeB magnet scrap proposed by U. S. Bureau of Mines.

consists of highly contaminated and oxidized fine powder or particulate in the particle size range of less than 50μm, and slag by using hydrofluoric acid.

Aqueous based technology can produce very high quality materials, even from swarf materials. However, this method involves a number of chemical extraction and reduction steps and requires the use of large amounts of dangerous solutions. Due to the complexity and expense of taking the metallic material, converting it to inorganic compounds, and then returning it to oxides or fluorides suitable for refining, this methodology is impractical for recycling purposes.

1.2.2 Electroslag refining

This process [10] is a method of treating rare earth-transition metal scrap contaminated with one or more tramp impurities, especially oxygen and nitrogen, picked up by the scrap from previous fabrication operations. The tramp impurities are reduced to concentrations acceptable for reuse of the treated alloy in the manufacture of end-use articles.

The various steps involved in this method are illustrated in Figure 2. Rare earth-transition metal scrap is typically received from one or more fabricating operations and initially segregated by alloy composition, size, shape, and other factors. Then scrap material is melted either as a consumable electrode or by addition to a molten bath and purified by contacting the scrap in the molten state with a suitable alkali halide flux or alkaline earth halide flux. The molten flux and the molten alloy react in the melting container in accordance with a typical slag / melt reaction between the molten flux and the molten alloy to remove tramp non-metallic impurities such as oxygen, nitrogen and hydrogen and metallic impurities such as Li, Na, Al, Si, Ca, Zn, Mg etc. from the molten alloy. The flux used is a prefused

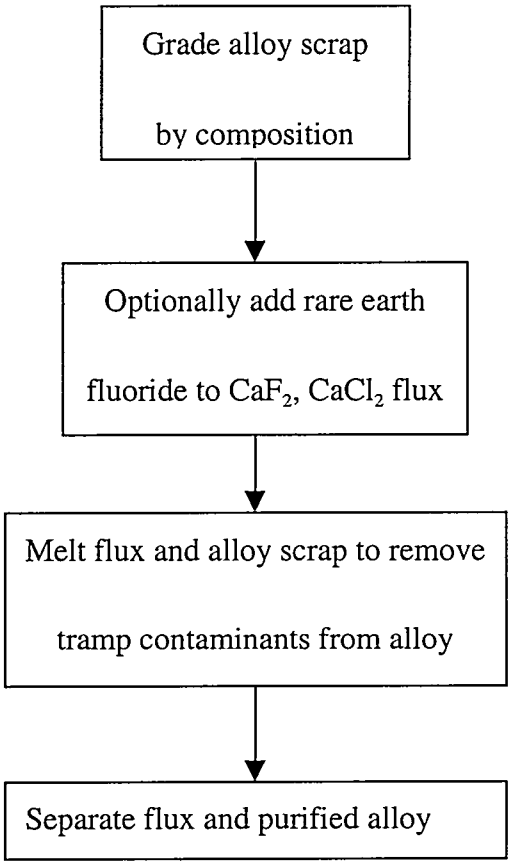

Figure 2. Electroslag refining of rare earth based scrap metals.

$CaCl_2$ / CaF_2 / RF_3 compound which was developed for the production of rare earth metals from their fluoride salts.

Electroslag refining is capable of treating a wide variety of binary, ternary and other rare earth-transition metal alloy scrap compositions e.g. Tb-Dy-Fe and Nd-Fe-B scrap. This method is an effective process for up-grading scrap in relatively large clean pieces. However, it does have some drawbacks. Firstly, this process is best suited for large, relatively clean, scrap materials such as magnets broken during manufacture or magnets that have been

rejected for use as a result of low magnetic strength or other defects. This process is not very effective on swarf materials due to their fine particulate nature and very high levels of contamination. Secondly, this process does not lend itself to the separation of the rare earth from the transition metal. This technology would not be suitable if a material is being recycled for either its rare earth or transition metal value as an input to the production of an unrelated alloy.

1.2.3 Fluxless melting method

The objective of this method [11] is similar to that of electroslag refining. Figure 3 is the flow sheet presenting the steps of this method. The scrap is melted and held in a bottom-pour refractory container at temperature conditions suitable to allow formation of dross. This dross forms as a result of the high reactivity of the rare earth element toward oxygen and nitrogen in the melt such as Nd_2O_3 and / or NdN for NdFeB magnet scrap and the relative insolubility of the resulting rare earth oxide and nitride compounds in the melt. The dross may also contain CaO, Al_2O_3, MgO etc. The dross floats on the melt because of its lower density. The dross can be further treated to recover a rare earth / iron fluoride compound useful as a reactant in the thermite reduction process or other metallothermic reduction processes. The purified melt is separated from the dross for reuse. Since the formation of the dross removes the rare earth constituent from the melt, the level of the rare earth constituent is brought up to the level desired in the final melt by addition of a master alloy of rare earth-transition metal while maintaining the overall melt chemistry within the desired range.

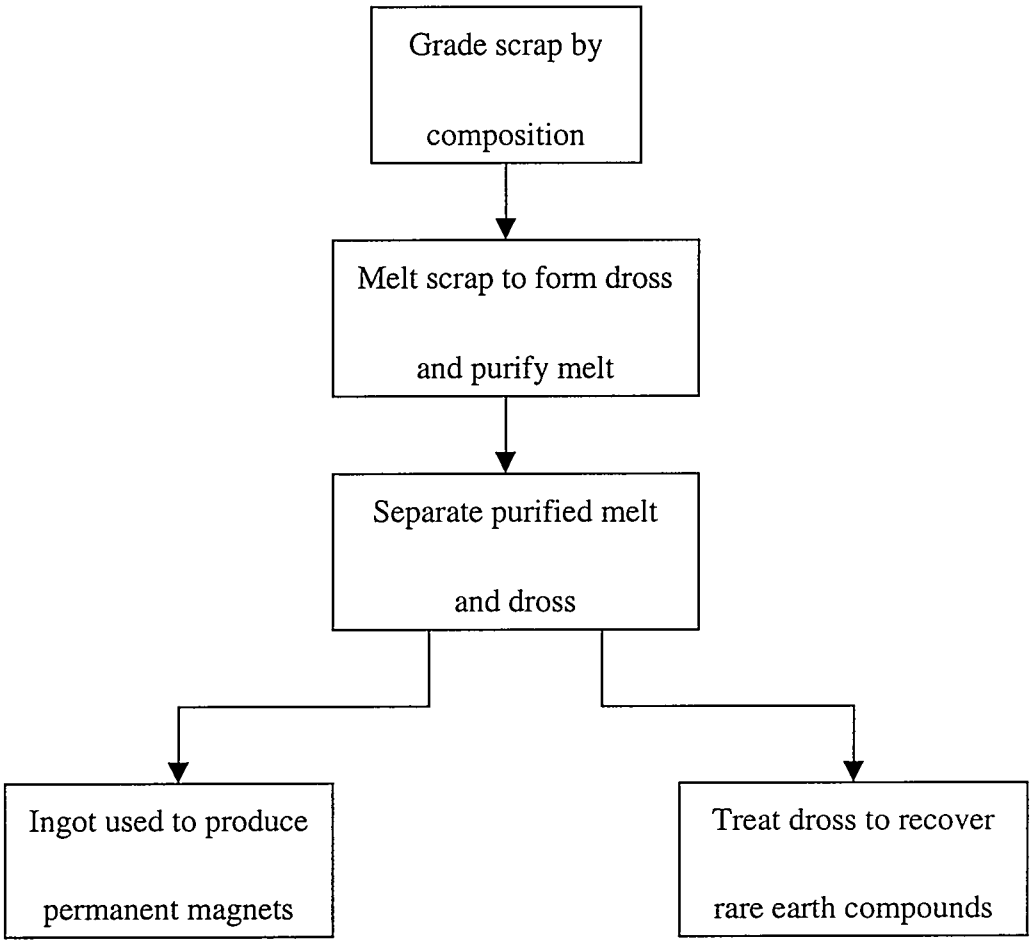

Figure 3. Flow sheet of fluxless melting method.

This method is advantageous in treating rare earth-transition metal scrap having oxygen in the range of about 0.5wt.% to about 0.75wt.% and nitrogen in the range of about 0.05wt.% to about 0.20wt.%.

1.3 Methods used in this investigation

The technique chosen for recycling Nd from NdFeB magnet scrap in this investigation is liquid metal extraction. Liquid metal extraction (LME) technology based on

liquid metal solvents is a common industrial operation. As the name implies, LME involves the partition of a solute between two phases that are immiscible in each other. Generally, at least one of the phases is liquid, the other a liquid or a solid. Liquid metal extraction has several advantages over other techniques. For example, it has the ability to handle a wide variety of scrap feed materials, from swarf to ingots; produce clean material, i.e. low carbon, nitrogen, oxygen and unwanted metallics; and eliminate having to return to primary metal reduction from a metal compound. One commonly used example of LME is the separation of silver from lead ores by a method known as the Parks process.

A. P. Bayanov [14] and R. Kontrimas [15] studied the extraction of rare earths (from lanthanum to lutetium) using a Zn - Pb melt. In this study they determined the distribution coefficient, $K_d = C_{Zn}/C_{Pb}$, where C_{Zn} and C_{Pb} are the equilibrium liquid Zn and Pb concentrations, for several rare earth and some transition metals. The distribution coefficient is related to temperature by

$$\log K_d = A + \frac{B}{T},$$

Where T is temperature and, A and B are constants. Their data are presented in Table 1. This process consisted of dissolution of the rare earth alloy by an alloy system in which the rare earth and other transition metals distribute themselves between the liquid phases where the liquid phases are not miscible in any proportions. The Zn rich and Pb rich liquids after dissolution are separated by density, and the dissolved metals were removed by a distillation / sublimation processing. The Zn and Pb could then be recycled back into the process.

A schematic of the liquid / liquid extraction circuit for the separation of La from Ni for recycling $LaNi_5$ alloys is shown in Figure 4. The extracted metals are removed by

Table 1. Distribution coefficient of rare earth and transition metals in liquid Zn - Pb alloy at 500°C with concentration measured in the liquid alloy.

Element	K_d	Element	K_d
La	5000	Ag	30
Ce	4000	Mn	200
Pr	6000	Au	3656
Nd	4000	Fe	>10000
Sm	3100	Co	>10000
Sn	0.500	Ni	>10000

vacuum distillation. Although the rare earth elements are strongly distributed to the Zn phase, so also are many of the transition elements. Therefore, the Zn / Pb system is not ideal for the separation of rare earth and transition metals.

Liquid metal extraction processing has been investigated by several research groups at Ames Laboratory in the early 1960's [12, 13]. In a cursory study [16] LME was used to remove both the Nd from $Nd_2Fe_{14}B$ alloys and Dy, Tb from $Dy_{0.25}Tb_{0.75}Fe$ alloys. The molten rare earth metal-bearing material and the molten extractant, such as Mg, Ca, Ba or other Group IIA metal in which the rare earth is soluble in the molten state, were in contact at a temperature and time effective to extract the rare earth metal from the melted material into the melted extractant. Although not attempted in this study, it was speculated that the rare earth metal with higher vapor pressure, e.g. Dy, Tb and Nd, can then be separated from the

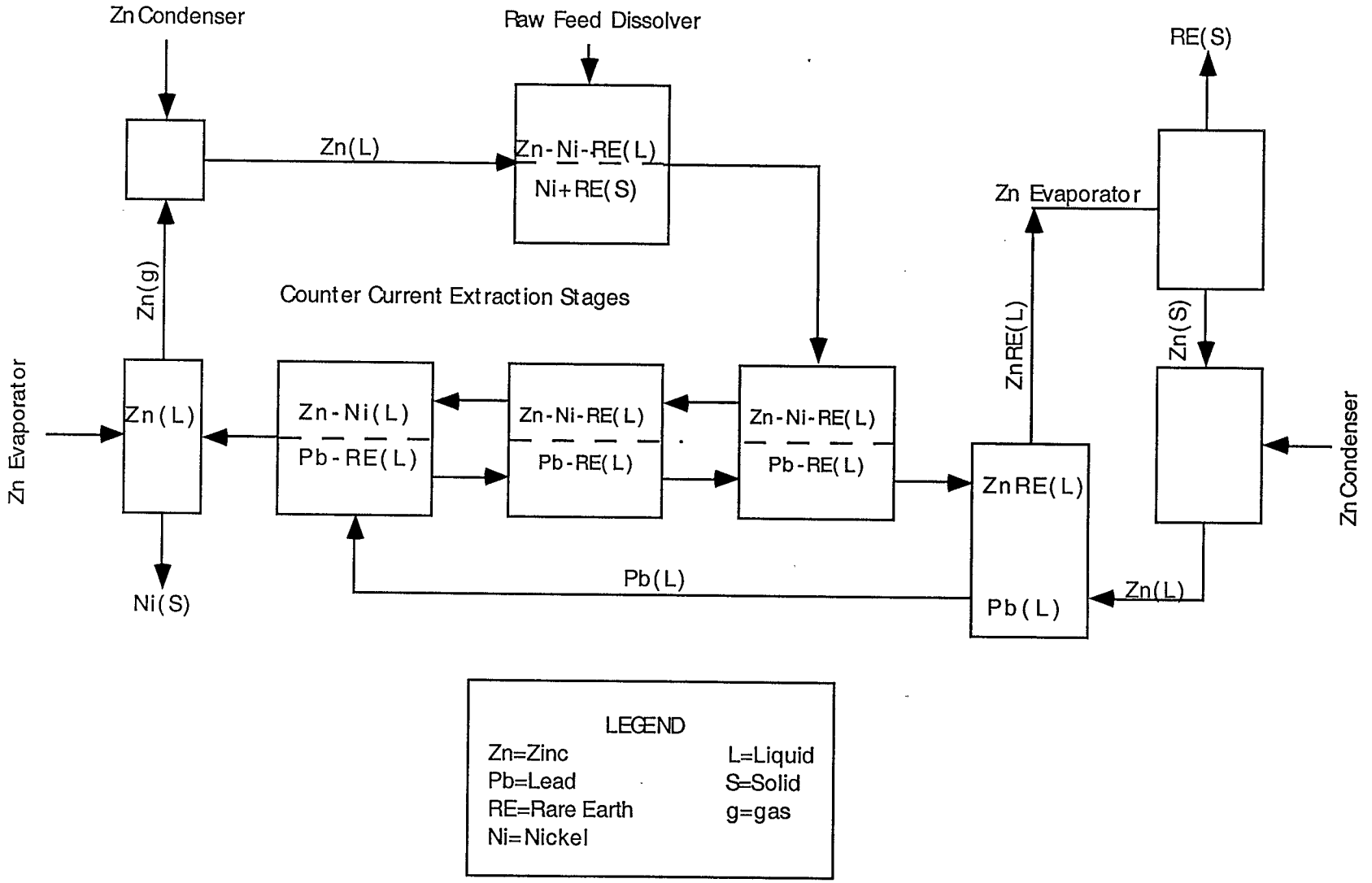

Figure 4. Schematic of Liquid / Liquid extraction circuit for the separation of La from Ni.

extractant with lower vapor pressure, e.g. Mg, by vacuum sublimation or distillation. The extractant can be recycled back into the process.

In summary, aqueous based recycling does not directly produce a metallic product but requires refining the metal by metallothermic reduction, which adds economic burden. Electroslag reprocessing does not require metallothermic reduction to produce metal, but the process is limited to relatively large pieces of clean scrap material, i.e. reprocessing of swarf is not feasible. Only liquid metal extraction using metallic solvents appears applicable to a wide variety of feed materials and allows the separation of metallic species without metallothermic reduction. However, more research and development is required before a commercial scale operation using this technique could be considered.

1.4 Statement of study

This study focused on liquid / solid extraction processing to recycle Nd from NdFeB magnet scrap. In this study liquid Mg was used as the extractant to remove Nd from NdFeB magnet scrap. Nd is soluble in liquid Mg and forms a number of intermetallic compounds while Fe and B are essentially immiscible in Mg. Therefore, liquid Mg readily takes up Nd, forming a Mg - Nd solution, while leaving the Fe and B unaffected. The phase diagrams of Mg - Nd and Mg - Fe are shown in Figure 5 and 6 [17].

The production of a Nd - rich alloy should find immediate application in the Mg casting industry, where rare earths are routinely added to improve mechanical properties. Magnesium alloys with rare-earth elements, e.g. neodymium, yttrium, together with zirconium exhibit improved creep resistance at elevated temperatures, reduced microporosity

in castings, and improved weldability [18]. The price of such castings currently is very high. For example, in a typical casting of QE22 containing only 2.2wt% Nd, the cost of the Nd accounts for over 40% of the cost of the raw materials [19]. These costs can be lowered if a master Mg - Nd alloy can be produced by an inexpensive recycling scheme. Thus, a successful extraction of Nd into Mg in a usable form will eliminate wastes and lower subsequent alloy casting costs as well.

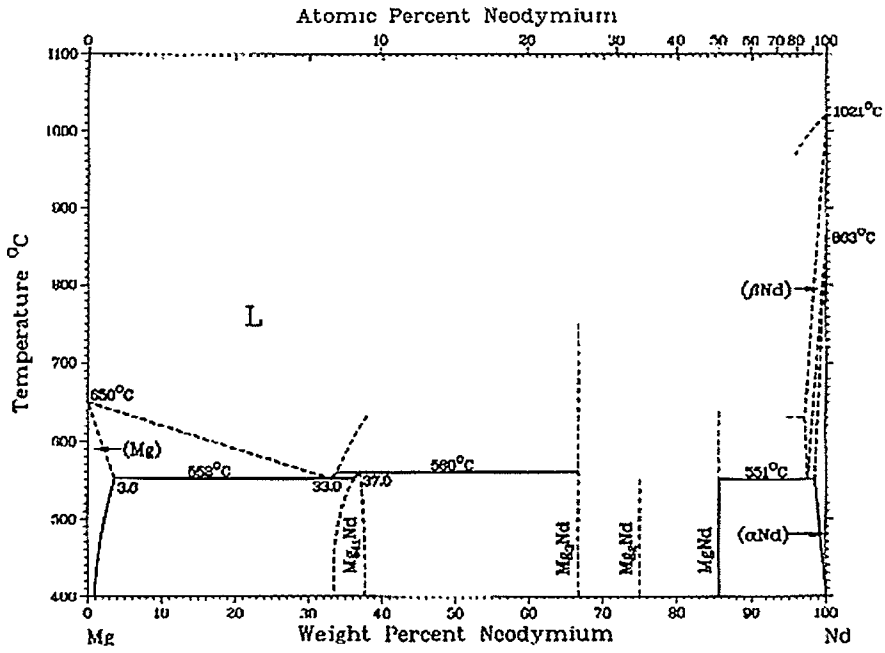

Figure 5. The phase diagram of Mg - Nd.

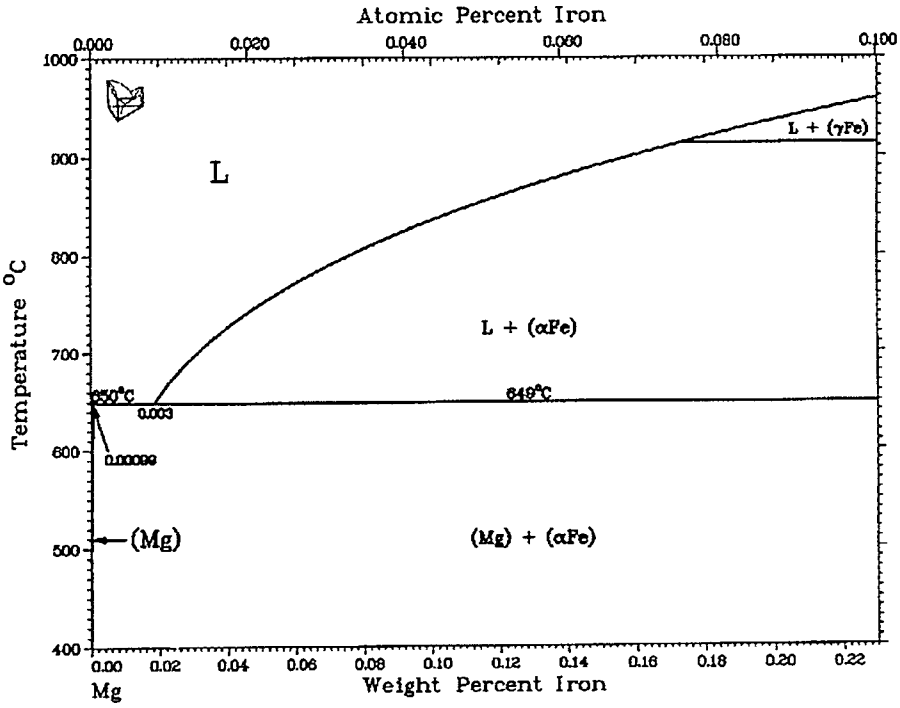

Figure 6. The phase diagram of Mg - Fe.

2 EXPERIMENTAL PROCEDURE

2.1 NdFeB magnet scrap

The starting material for this experiment consisted of large irregularly shaped pieces of magnet scrap produced by powder processing. The average composition of the scrap as determined by chemical analysis of test samples is shown in Table 2.

Table 2. Overall composition of NdFeB magnet scrap. Nd, Fe, B, Pr, and Dy given in weight percent, C, N, and O given in parts per million.

Nd (±1.0)	Fe (±0.7)	B (±0.04)	Pr (±0.01)	Dy (±0.3)	C	N	O
18.0	72.4	0.90	1.82	5.3	0.0336	29	343

The purity of magnesium used was 99.8% (metal basis). The NdFeB scrap was placed in a 5.0cm diameter × 10.0cm high stainless steel crucible along with pieces of pure Mg in an argon atmosphere dry box. The general geometry and size of the pieces is shown in Figure 7. The size of each scrap piece was larger than 10mesh. The crucibles were induction heated using a 25KW, 3000Hz LEPEL generator in an atmosphere-controlled chamber to temperatures ranging from 675°C – 750°C for times ranging from 2 – 8 hours. The complete listing of the samples studied is shown in Table 3. The temperature was measured continuously by Pt - 13% Rh thermocouple. Before heating the chamber was evacuated then back-filled with Ar whose purity was greater than 99% to maintain a clean environment and

minimize oxidation and vaporization of the Mg. The weight loss of the cast samples was due to the possible vaporization of magnesium and residual magnesium which stuck to the thermocouple, while weight gain of the cast samples can be explained by slight oxidation of the magnesium at the top of the crucible upon cooling.

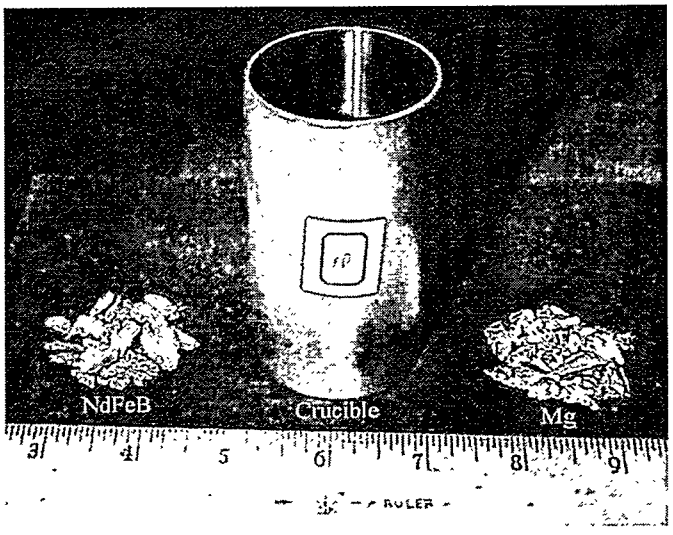

Figure 7. The geometry of NdFeB magnet scrap, pure Mg, and stainless steel crucible.

After being held at the pre-determined temperature for the specified time, the crucibles were cooled, and the molten Mg was allowed to solidify in the crucible. The crucibles were then cross-sectioned and polished for analysis. Characterization of the cast samples was carried out using a scanning electron microscope (SEM) equipped with energy dispersive spectroscopy (EDS), X-ray diffraction (XRD), and chemical analysis using Inductively Coupled Plasma (ICP). The thickness of the diffusion layer was measured from backscattered image of SEM. The phase determinations were made based on X-ray diffraction scans.

Table 3. List of casting temperature / time and weight of NdFeB magnet scrap.

Sample Number	Casting Temp/Time	Weight of crucible (gram)	Weight of NdFeB scrap (gram)	Weight of Mg (gram)	Total Weight of sample before casting, W_b (gram)	Total Weight of sample after casting, W_a (gram)	W_a-W_b (gram)	Weight gain/loss (%)
1	675°C/8h	215.3	50.0	161.9	427.2	425.6	-1.6	-0.37
2	700°C/2h	215.3	50.0	162.2	427.5	424.7	-2.8	-0.66
3	700°C/4h	218.2	50.0	161.8	430.0	431.7	+1.7	+0.39
4	700°C/8h	216.2	50.0	161.9	428.1	427.4	-0.7	-0.16
5	725°C/2h	215.1	50.0	110.8	376.5	377.2	0.7	0.18
6	725°C/8h	216.0	50.0	161.8	427.8	429.2	+1.4	+0.33
7	750°C/2h	215.5	50.0	159.5	425.0	425.6	+0.6	+0.14
8	750°C/4h	215.7	50.0	162.8	428.5	429.0	+0.5	+0.12
9	750°C/8h	217.8	50.0	166.0	433.8	431.2	-2.6	-0.60

2.2 NdFeB magnet particulate

The material used for these experiments was different size irregularly shaped NdFeB magnet particulate produced by powder processing. The average composition and sizes of the particulate are shown in Table 4.

The casting temperature / time and weight of each sample are shown in Table 5. The subsequent analysis procedures for the castings were the same as for NdFeB magnet scrap (see section 2.1).

Table 4. Overall composition of NdFeB magnet particulate. All elements are given in weight percent.

NdFeB Particulate	Nd (±0.4)	Fe (±3)	B (±0.01)	Pr (±0.014)	Dy (±0.2)	C	N	O
20 mesh	24.2	72	0.80	1.443	7.0	0.0365	0.0023	0.0241
30 mesh	24.2	72	0.82	1.437	7.0	0.0437	0.0024	0.1112
+50 mesh	24.2	71	0.80	1.401	7.0	0.0358	0.0032	0.0731
-50 mesh	24.1	71	0.82	1.385	6.9	0.0410	0.0072	0.2234

Table 5. List of casting temperature / time and size of NdFeB magnet particulate.

NdFeB particulate	Casting Temp/Time	Weight of crucible (gram)	Weight of NdFeB scrap (gram)	Weight of Mg (gram)	Total Weight of sample before casting, W_b (gram)	Total Weight of sample after casting, W_a (gram)	W_a-W_b (gram)	Weight gain/loss (%)
20 mesh	750°C/4h	217.6	50.0	118.8	387.0	385.9	-1.1	-0.28
30 mesh	750°C/4h	217.2	50.0	116.4	384.2	382.7	-1.5	-0.39
+50 mesh	750°C/4h	217.3	50.0	118.9	386.7	386.4	-0.3	-0.08
-50 mesh	750°C/4h	217.6	50.0	52.6	320.4	319.4	-1.0	-0.31

3 EXPERIMENTAL RESULTS

3.1 NdFeB magnet scrap

3.1.1 Microstructure of the NdFeB scrap and diffusion region

A typical cast sample is shown in Figure 8. The constituents of the casting, namely the now solidified Mg and the scrap NdFeB pieces, are clearly seen. Figures 9a and 9b show the diffusion region. Figure 10 is a series of high magnification micrographs showing the phases present in the various regions across the transition zone from the unaffected NdFeB / diffusion layer to the diffusion layer / solidified Mg interface.

Close observation of the sample using backscattered electron imaging (BSE) reveals that the scrap consists of three distinct zones. The compositions of these phases are shown in Table 6. Note that due to the difficulty of using EDS to quantitatively determine B (which is only present in small amounts), this element is not listed. The identifications made in Table 6 are based on the relative amounts of Nd and Fe detected and the phases known to commonly exist in NdFeB magnet materials [20 - 22]. Upon this basis, the light gray phase that constitutes the matrix of the magnet material and marked as "1" in Figure 10a is identified as $Nd_2Fe_{14}B$, while the medium gray phase is Nd_2Fe_{17} ("2" in Figure 10a). The third phase ("3" in Figure 10a) has only minor amounts of Nd and is identified as α-Fe with some Nd in solid solution. In the transition region shown in Figure 10b a Nd depleted region exists where diffusion of the Nd from the scrap has occurred. The same phases are observed in this region, namely, $Nd_2Fe_{14}B$, Nd_2Fe_{17}, and α-Fe + Nd, although now α-Fe + Nd is the dominant phase in the diffusion layer. The diffusion layer / solidified Mg interface is shown in Figure 10c.

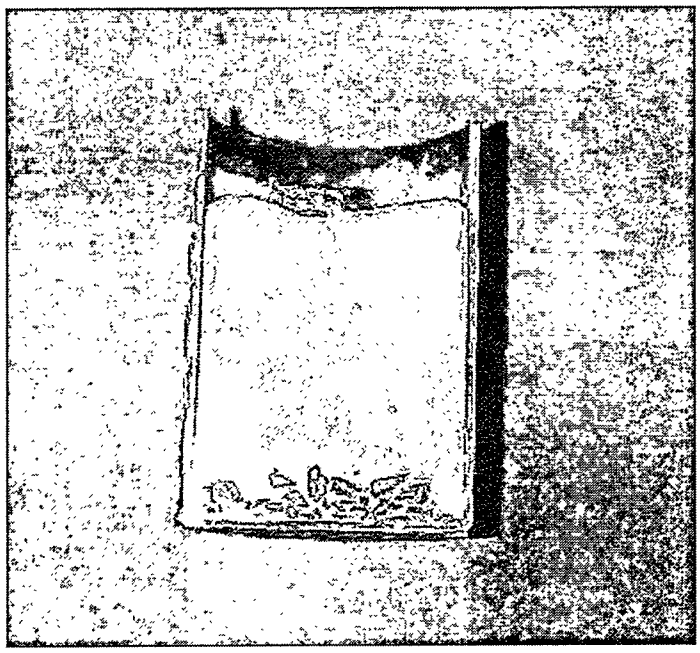

Figure 8. Macrostructure of the sample cast at 700°C for 4 hours.

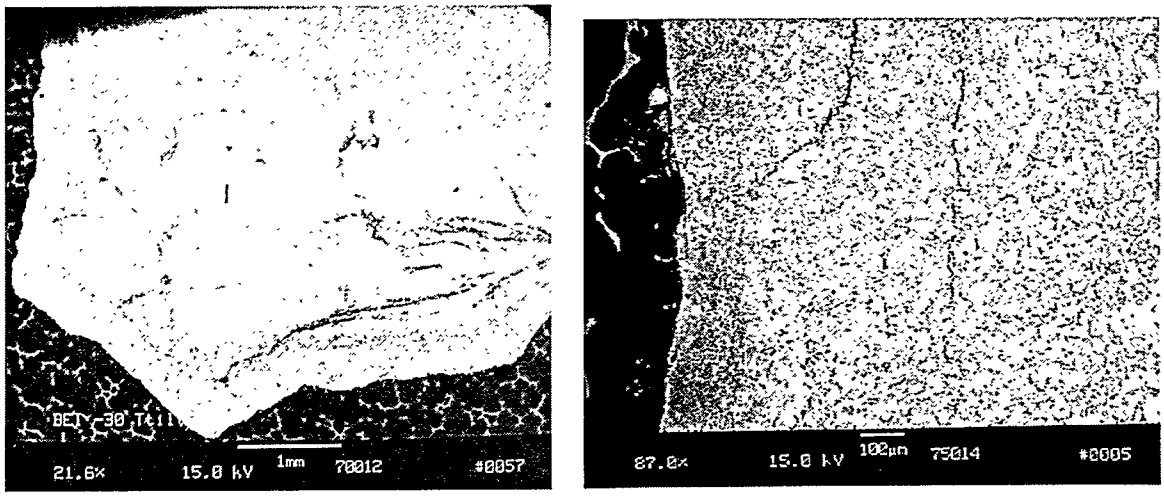

(a) (b)

Figure 9. (a) Microstructure of the cast sample,

(b) The diffusion layer observed in NdFeB scrap.

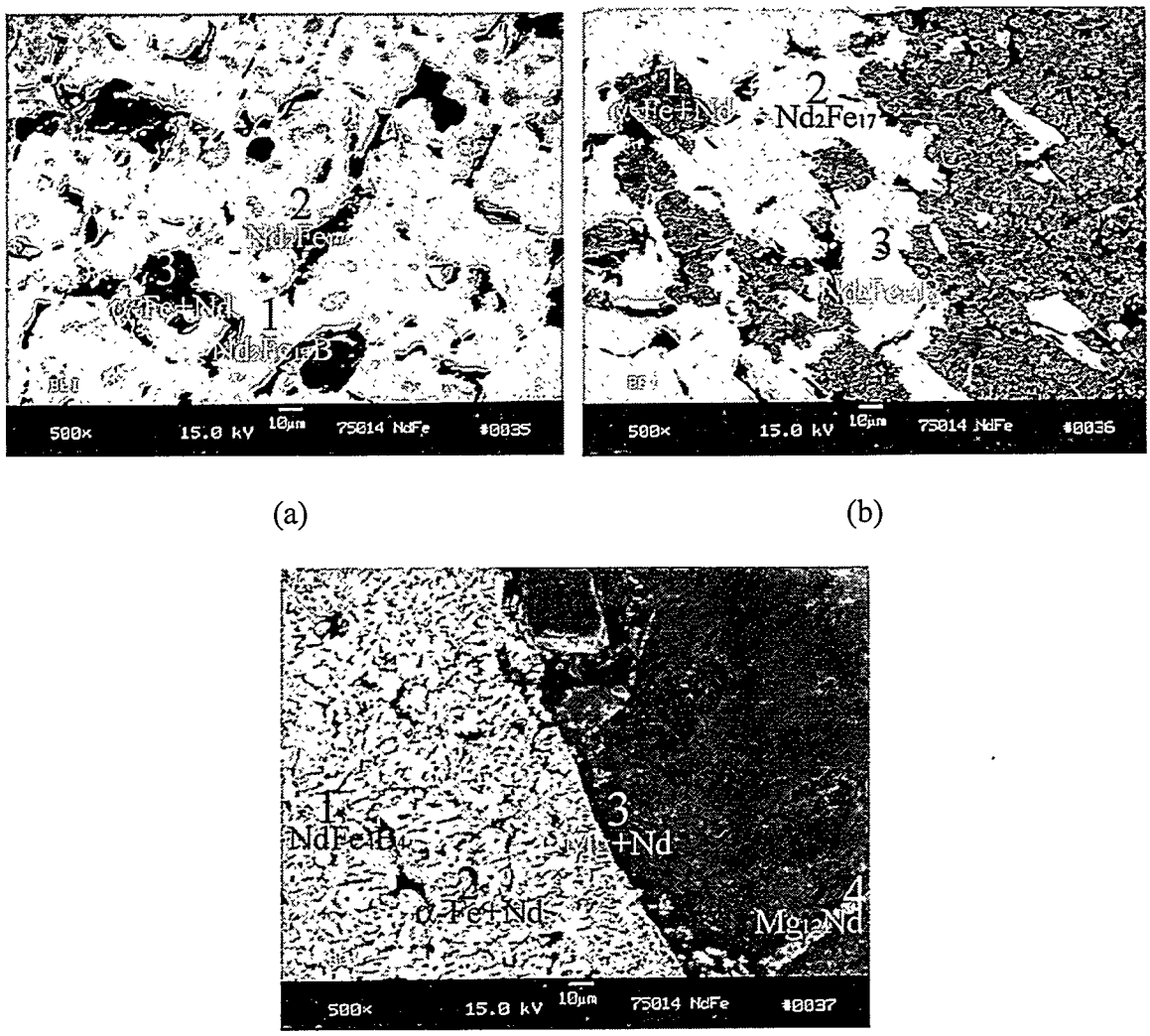

(a) (b)

(c)

Figure 10. Micrographs showing the various regions from unaffected NdFeB scrap to solidified Mg.

(a) Unaffected NdFeB scrap,

(b) Interface between unaffected and diffusion depleted zone in solid scrap,

(c) Interface between diffusion depleted zone and solidified Mg + Nd.

Table 6. The EDS results and phase analysis. The * data indicates questionable data.

Figure 10 Micrographs		Composition (wt.%)			Phase	Description
		Nd ±0.40	Fe ±0.35	Mg ±0.50		
(a) NdFeB	Spot 1	22.48	77.52	- -	$Nd_2Fe_{14}B$	Light Gray
	Spot 2	17.82	82.18	- -	Nd_2Fe_{17}	Medium Gray
	Spot 3	0.73	99.27	- -	α-Fe+Nd	Dark Gray
(b) Scrap / Diffusion Layer	Spot 1	0.33*	99.67	- -	α-Fe+Nd	Dark Gray
	Spot 2	17.90	82.10	- -	Nd_2Fe_{17}	Medium Gray
	Spot 3	21.45	78.55	- -	$Nd_2Fe_{14}B$	Light Gray
(c) Diffusion Layer / Solidified Mg	Spot 1	36.34	63.66	- -	$NdFe_4B_4$	White
	Spot 2	0.45*	99.55	- -	α-Fe+Nd	Medium Gray
	Spot 3	2.1	1.9	96.0	Mg+Nd	Dark Gray
	Spot 4	34.92	0.28*	64.8	$Mg_{12}Nd$	Light Gray

The major phase is again α-Fe + Nd in the diffusion zone. Near the interface, but within the α-Fe + Nd diffusion zone a few small white particles can be seen. These particles are identified as $NdFe_4B_4$. The composition changes abruptly at the interface as the now solidified Mg becomes the matrix phase. Although Mg and Fe are essentially immiscible, right at the interface a small amount of Fe was detected, along with Nd in solid solution. However, the low values detected are less than one standard deviation away from the

measured mean. Therefore, statistically they are considered non-definitive and are subject to question.

3.1.2 Microstructure of the solidified magnesium matrix

The microstructure of the solidified Mg consists of grains of Mg with a Nd-rich intermetallic phase present at the grain boundaries, Figure 11a. Within the grains a fine plate-like Widmanstatten structure is observed, Figure 11b. Wide area X-ray EDS analysis revealed that the matrix contains Nd present in solid solution in amounts up to 3.0wt.%. The phase distributed on the grain boundaries contains ≈ 32-36wt.% of Nd, (e.g. Spot 4, Table 6) and is identified as $Mg_{12}Nd$. Although the needles are too small for accurate EDS analysis (Table 7), being less than 0.1μm in thickness, the Mg - Nd phase diagram (Figure 5) predicts that upon cooling $Mg_{12}Nd$ will precipitate from a supersaturated solid solution. This agrees with BSE observations since they possess the same contrast level as the intergranular $Mg_{12}Nd$ easily identified using EDS.

X-ray diffraction scans of the matrix were run to confirm this identification. A typical spectrum obtained from the center of the casting away from the scrap pieces is shown in Figure 12 with a listing of the observed peaks shown in Table 8. All of the peaks in the XRD scans could be identified as either Mg or $Mg_{12}Nd$.

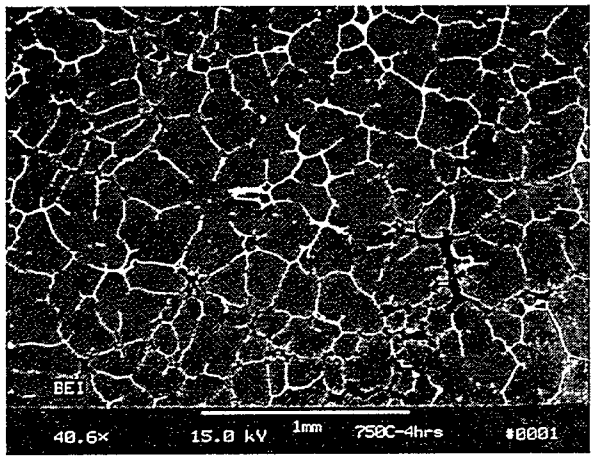

(a)

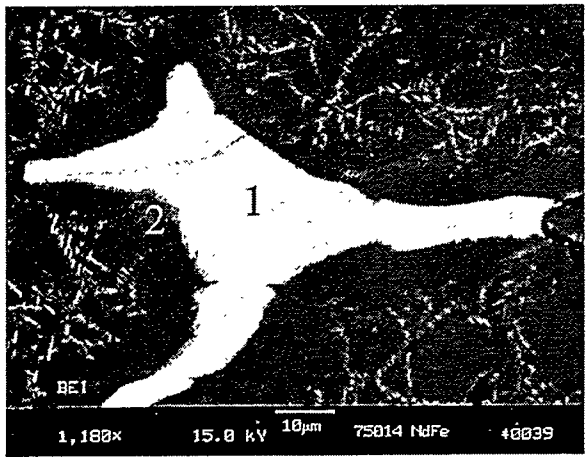

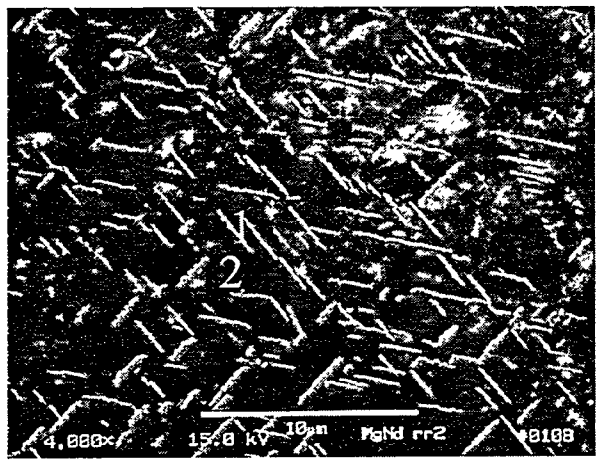

(b) (c)

Figure 11. Microstructure of molten Mg in the cast condition.

(a) Overall appearance of the matrix,

(b) Close-up showing the intergranular phase,

(c) Close-up showing the Widmanstatten structure.

Table 7. The EDS results of Figure 11.

Figure 11 Micrographs		Composition (wt.%) Nd ±0.40	Mg ±0.50	Phase	Description
(b) Intergranular phase	Spot 1	33.96	66.04	$Mg_{12}Nd$	Bright
	Spot 2	3.20	96.80	α-Mg+Nd	Dark Gray
(c) Widmanstatten structure	Spot 1	7.42	92.58	$Mg_{12}Nd$	Bright Needle
	Spot 2	3.04	96.95	α-Mg+Nd	Dark Gray Between Needles

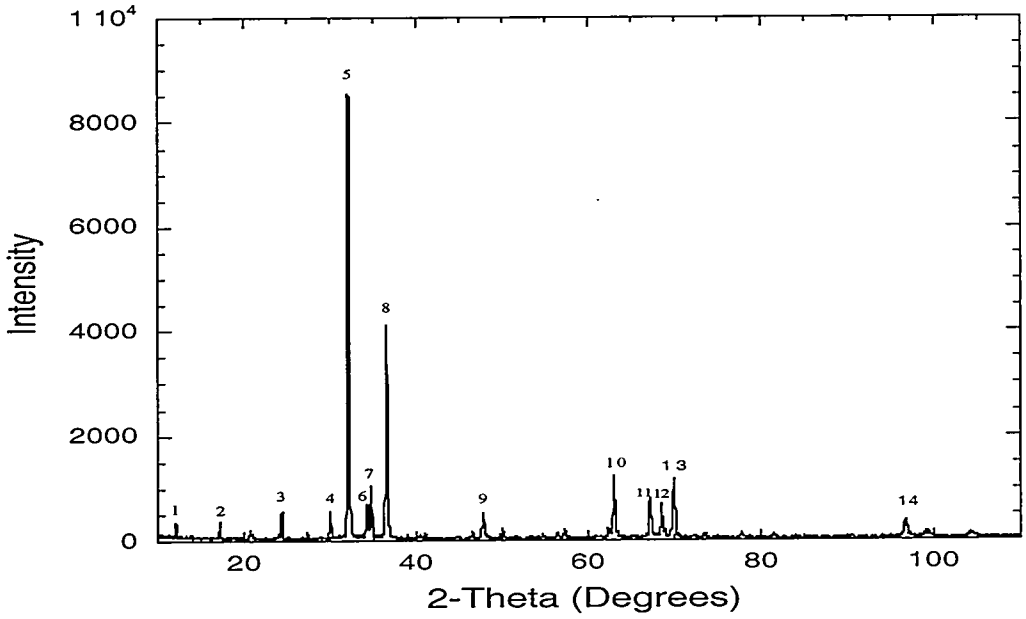

Figure 12. X-ray diffraction scan of solidified Mg + Nd.

Table 8. Indices of each X-ray peak of solidified Mg + Nd.

Peak Number	2θ	Mg (h k l)	$Mg_{12}Nd$ (h k l)	Peak Number	2θ	Mg (h k l)	$Mg_{12}Nd$ (h k l)
1	12.0968		1 1 0	8	36.5487	1 0 1	
2	17.1809		1 0 1	9	47.7672	1 0 2	
3	24.3965		2 1 1	10	63.0056	1 0 3	
4	30.0117		3 0 1	11	67.0932	2 0 0	
5	32.0223	1 0 0		12	68.5282	1 1 2	2 2 4
6	34.3376	0 0 2		13	69.8362	2 0 1	3 1 4
7	34.7538		2 0 2	14	96.6355	2 1 1	

3.1.3 Chemical composition

Results of the chemical analysis by ICP of molten magnesium are shown in Table 9. All samples showed low impurity values in the Mg with substantial gain of Nd from the scrap material. While all the samples had approximately the same amount of scrap + Mg, the amount of Nd in the casting should only be considered for qualitative comparisons. A number of factors such as time, temperature, surface area of the scrap, location of the sample used for ICP etc. must be considered before making accurate quantitative comparisons. In general the percentage of Nd increases with time and temperature.

Table 9. Chemical composition analysis of molten magnesium with NdFeB magnet scrap.

Sample Number	Casting Temperature/Hours	Chemical Composition						
		Nd (wt.%)	Mg (wt.%)	Fe (wt.%)	B (wt.%)	C (ppm)	N (ppm)	O (ppm)
1	675°C/8h	0.54±0.02	94.1±0.7	0.0141±0.0008	ND	79	<1	52
2	700°C/2h	2.72±0.11	98.0±4.0	0.0418±0.0014	<0.0018	32	<1	105
3	700°C/4h	3.88±0.04	96.0±3.0	0.044±0.001	<0.009	110	12	71
4	700°C/8h	3.74±0.06	96.0±3.0	0.049±0.001	<0.009	60	<1	100
5	725°C/2h	5.6±0.18	91.2±0.7	0.034±0.0006	ND	110	<1	21
6	725°C/8h	4.7±0.2	92.1±0.7	0.036±0.0007	ND	119	<1	16
7	750°C/2h	2.29±0.08	97.0±3.0	0.0713±0.0016	<0.009	52	<1	255
8	750°C/4h	3.90±0.14	96.0±3.0	0.052±0.002	<0.0018	69	<1	176
9	750°C/8h	3.57±0.09	97.0±4.0	0.101±0.005	<0.013	174	68	139

3.2 NdFeB magnet particulate

3.2.1 Microstructure of the NdFeB magnet particulate + solidified Mg

SEM observations of the cast samples, i.e. the constituents of solidified Mg and irregular NdFeB particulate, reveal that most of the particulate was free of Nd (Figure 13c, 13d). However, some larger particles showed a two-phase structure indicative of a diffusion layer within the particles (Figure 13a), although some smaller particles showed a mottled two-phase structure (Figure 13b). It is believed that smaller particles possessed an oxide film that slowed the diffusion process. The EDS results and phase analysis of the cast samples are shown in Table 10. This result is consistent with the phase identification of NdFeB magnet scrap.

3.2.2 Chemical composition

Results of the chemical analysis of molten magnesium are shown in Table 11. All samples showed substantial gain of Nd from the particulate material and relatively higher impurity values such as carbon, nitrogen and oxygen than those in molten magnesium cast with scrap material.

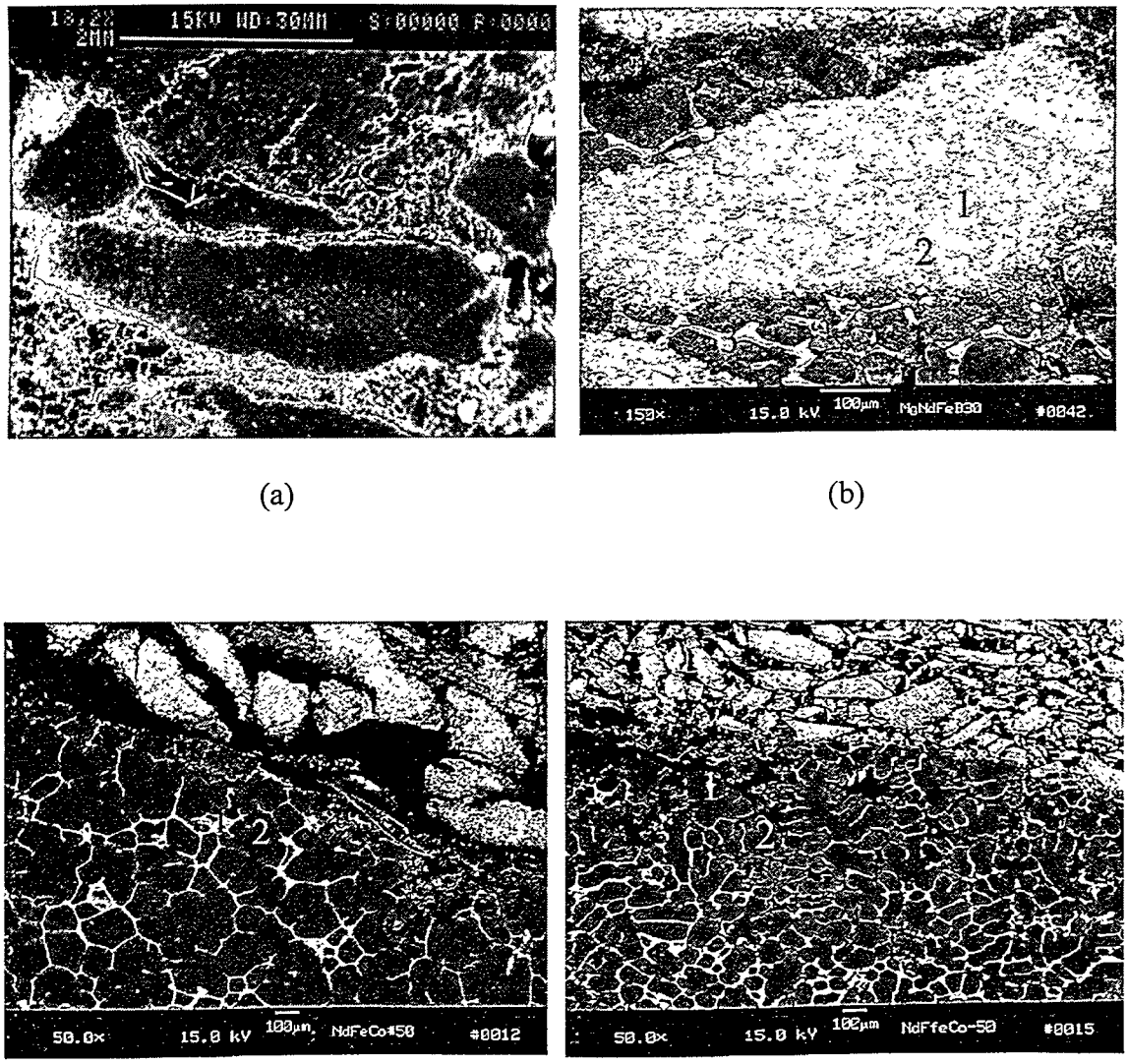

Figure 13. SEM micrographs of molten Mg with (a) 20mesh, (b) 30mesh, (c) +50mesh, (d) -50mesh NdFeB particulate.

Table 10. The EDS results and phase analysis. The * data indicates questionable data.

Figure 13 Micrographs		Composition (wt.%)			Phase	Description
		Nd ±0.40	Fe ±0.35	Mg ±0.50		
(b) 30 mesh	Spot 1	27.16	64.49	8.35	$Nd_2Fe_{14}B$	Light Gray
	Spot 2	3.10	79.07	17.83	α-Fe+Nd	Medium Gray
	Spot 3	27.50	0.17*	72.33	$Mg_{12}Nd$	Gray
(c) +50 mesh	Spot 1	26.68	- -	73.32	$Mg_{12}Nd$	Bright
	Spot 2	1.46	0.03*	98.52	α-Mg+Nd	Dark Gray
(d) –50 mesh	Spot 1	26.72	- -	73.28	$Mg_{12}Nd$	Bright
	Spot 2	1.51	0.09*	98.40	α-Mg+Nd	Dark Gray

Table 11. Chemical composition analysis of molten magnesium with NdFeB magnet particulate.

NdFeB particulate	Chemical Composition (wt.%)								
	Mg	Nd	Fe	B	C	N	O	Pr	Dy
20 mesh	89.5±0.5	8.5±1.0	0.0639±0.0015	<0.02	0.0113	0.0011	0.0150	0.342±0.004	1.2±0.4
30 mesh	93.0±0.3	8.6±0.5	0.0414±0.0013	<0.01	0.0054	<0.0001	0.0210	0.312±0.003	1.0±0.2
+50 mesh	94.6±0.3	5.1±0.5	0.0470±0.0007	<0.01	0.0057	<0.0001	0.0098	0.167±0.002	0.5±0.2
-50 mesh	88.9±0.3	9.7±0.5	0.0427±0.0012	0.01	0.0028	<0.0001	0.0208	0.292±0.003	0.8±0.2

4 DISCUSSION

The phase diagram for Mg - Nd is shown in Figure 5 [17]. While numerous Mg - Nd phases have been identified, the exact nature of the phase diagram is still unknown. From observation of the microstructure it appears that the high affinity of Mg for Nd causes Nd to rapidly diffuse out of the solid NdFeB magnet scrap and into the liquid at high temperatures. While the amount of Nd present in the matrix depends on hold time and temperature and varies for each casting, chemical analysis of the once molten Mg matrices with NdFeB scrap (Table 9) shows that on average the total Nd content falls near the solid solubility limit of Nd in Mg, around 3 - 4wt.%. The average total Nd content in the once molten Mg matrix with NdFeB particulate is around 8 - 9wt. %. The increase in total Nd content is due to the reduced amount of Mg cast with NdFeB particulate material. Upon solidification, Mg grains nucleate and grow, becoming enriched in Nd as solidification proceeds. At the eutectic temperature the composition of the remaining liquid approaches that of the intermetallic compound $Mg_{12}Nd$. This phase nucleates and grows on the grain boundaries upon solidification. As the Nd supersaturated Mg matrix cools, the intermetallic also nucleates and precipitates within the Mg grains in the form of a Widmanstatten structure.

4.1 Diffusion of Nd through NdFeB scrap

The thickness of the diffusion layer was determined by making a number of measurements on SEM micrographs and averaging the results. Since the scrap particulate was of irregular size and shape and spaced randomly within the crucibles, differences in sectioning of the particles during polishing is expected. Any section not made perpendicular

to the diffusion direction will result in the diffusion zone appearing wider than what actually exists. In order to minimize this effect, measurements were obtained only from large particulate where the diffusion zone appeared of relatively constant thickness around the diameter, the assumption being that these zones most closely approach the actual width of the diffusion layer. This method assures that, at worst, the measured diffusion layer thickness will be slightly overestimated. Figure 14 shows a plot of the mean diffusion layer thickness at 700°C, 725°C and 750°C. Since only one sample was cast at 675°C, it is not shown in this Figure.

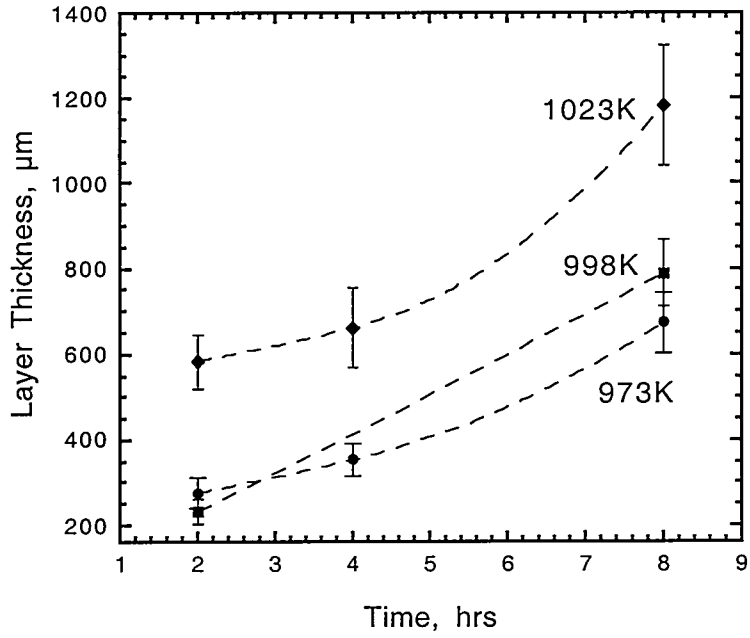

Figure 14. Diffusion layer thickness as determined from SEM micrographs at 973K, 998K and 1023K.

An automated EDS line scan was run beginning in the unaffected NdFeB scrap, through the diffusion layer, and into the Mg matrix for the sample cast at 725°C for 8 hours. The total length of the line scan was 1500μm, with the composition being sampled every 3.75 μm for a total number of 400 steps. The spectra were acquired for 200 seconds, and the data analyzed using a standards analysis. The composition profile is shown in Figure 15 and the complete set of data is listed in appendix. There are two important things that must be noted. Firstly, the compositions listed in this figure are based solely on a measurement of the Fe, Nd, and Mg X-rays collected from the sample. B could not be detected reliably, and the Pr and Dy known to be in the sample were ignored for this study. This causes the measured composition of Nd in the scrap, when normalized to one, to be closer to 27.0wt% than the overall composition of 18.0wt% determined by ICP. Secondly, there are many high-Nd points in Figure 15. These points originate from the high Nd content phases identified optically that are distributed throughout the NdFeB scrap, the diffusion zone, and the solidified Mg. For example, in the diffusion zone small remnant regions of the starting material are seen as is the intermetallic phase Nd_2Fe_{17}. In the Mg matrix the intermetallic $Mg_{12}Nd$ can be seen optically both interdendritically and as part of the Widmanstatten structure. These regions cause outlying points in the EDS data as the line scan crosses them. Ignoring these points, curves can be fit to the three distinct regions comprised by the NdFeB scrap, the diffusion layer, and the Mg matrix. These are shown in Figure 16. Note that for the diffusion region, the points having Nd content > 5wt.% were ignored since these were observed to be intermetallic compounds. Similarly, the points having Nd content higher or lower than 27wt.% were ignored in the unaffected scrap for the same reason. The scrap and diffusion zone regions exhibit linear curve fits while the solidified Mg fits well to a

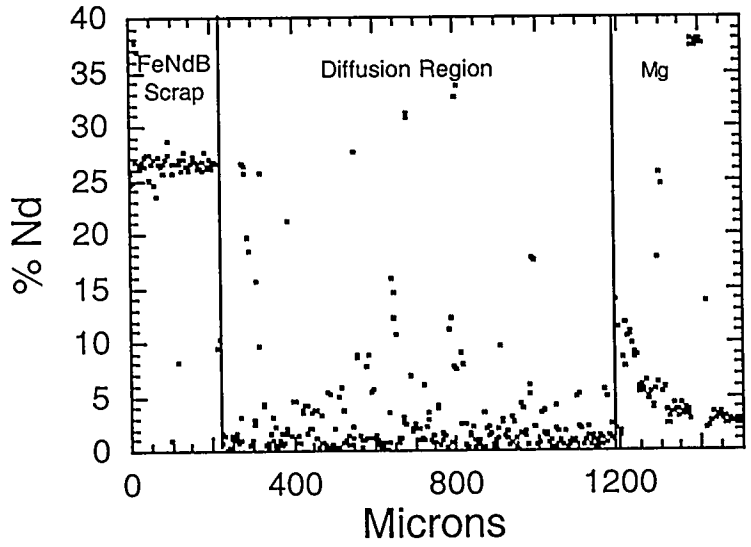

Figure 15. The composition profile for Nd across the diffusion layer.

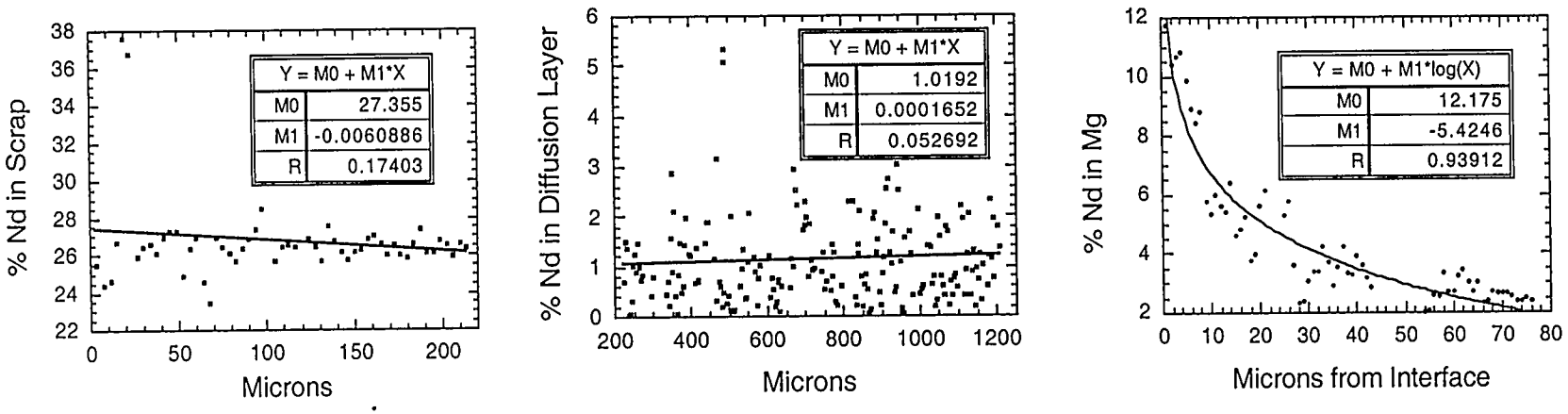

Figure 16. The fitted curves for Nd concentration profile for the three regions across the diffusion layer.

logarithmic curve. From these data the average composition of Nd in the scrap (excluding the contribution of Pr, Dy, and B) is ≈ 27.4wt.% Nd. The diffusion region is remarkably low in Nd, being ≈ 1.0wt.%. In order to account for the presence of the Pr, Dy, and B, a simple ratio comparing the %wt.Nd in the EDS scans to the more accurate value determined by ICP can be made. When this is done the wt.% Nd in the diffusion region falls to 0.67wt.%.

According to the Nd concentration profile across the diffusion layer obtained from the EDS line scan, the mass transport in the system can be described by making the following two assumptions:

Assumption 1: The solid / liquid interface remains fixed at the position it had at the start of the experiment. Since Fe can not dissolve into the Mg, it remains as a matrix through which the Nd is diffusing. As the Nd diffuses into the liquid, a two-phase zone which contains very little Nd is generated at the interface. Let the composition in this zone be designated Cz. While two-phase zones do not occur in binary systems, this system can be thought of as a ternary between the magnet scrap, the magnesium, and the Fe-rich diffusion zone. Thus, a two-phase region can form. The driving force for the diffusion of the Nd through the two-phase zone is the chemical potential gradient of Nd. Most of the Nd in the two-phase zone must be tied up as a compound with Fe (Nd_2Fe_{17}). In fact, small compounds are seen optically and can be identified in the EDS line scan. So the first assumption is that the average composition in the two-phase zone remains constant at Cz.

Assumption 2: During the casting process, significant convection occurs in the liquid Mg that remains relatively constant. The sources of convection include the thermal convection due to the horizontal temperature gradients inherent in a crucible heated from the sides and solute convection due to the horizontal composition gradient. So the second

assumption is that the thickness of the boundary layer in liquid Mg at the interface δ remains constant during the casting process, and the liquid Mg has a uniform composition C_l which will rise during the casting process.

With the above two assumptions, the diffusion process is schematically shown in Figure 17. The Nd flux out of the scrap (F_1) and the Nd flux into the liquid Mg (F_2) must be equal because all of the mass of Nd being removed from the NdFeB scrap ends up in the liquid Mg, i.e. F_1=F_2. The values for F_1 and F_2 can be written as [24, 25]:

$$F_1 = (C_s - C_z)\frac{dL}{dt} \quad (1)$$

$$F_2 = D\left(\frac{dC}{dZ}\right)_i \approx \left(D_0 e^{-Q/RT}\right)\frac{C_i}{\delta} \quad (2)$$

$$F_1 = F_2 \quad (3)$$

Where F_1: the flux out of the NdFeB scrap into the two-phase zone,

F_2: the flux out of the two-phase zone into the liquid Mg,

Cs: the average composition of Nd in the NdFeB scrap,

Cz: the average composition of Nd in the two-phase zone,

L: the average thickness of the diffusion zone,

t: holding time at temperature T,

D: the temperature dependent diffusion coefficient of Nd in liquid Mg,

D_0: temperature independent constant, known as the frequency factor.

Q: the activation energy,

R: 8.3143 J/K•mol,

C_i: the composition of Nd in liquid Mg at the solid / liquid interface,

δ: the thickness of the boundary layer in liquid Mg at the solid / liquid interface.

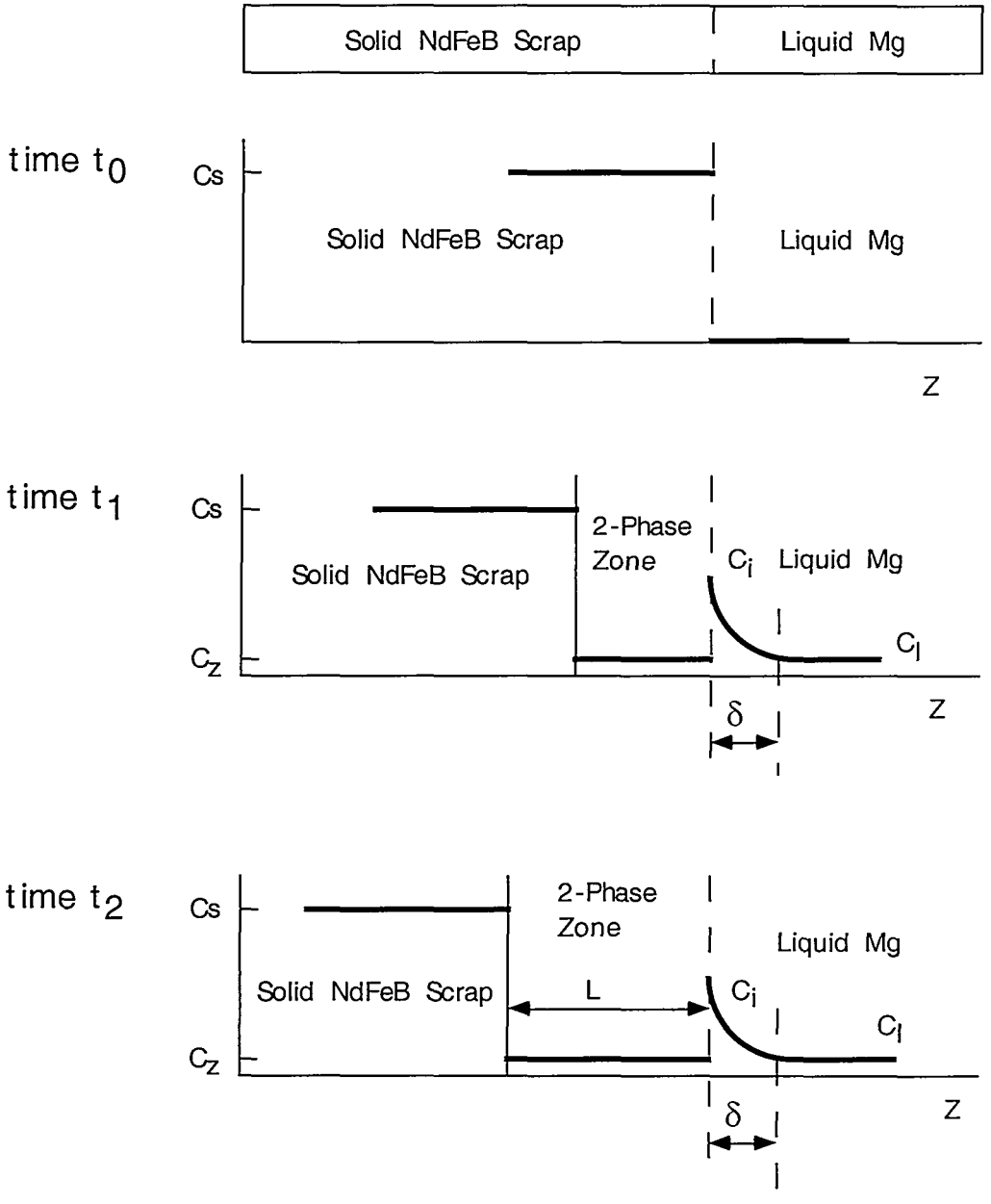

Figure 17. Schema indicating the mass transport process of the Nd from NdFeB scrap to liquid Mg, a two-phase zone is formed in this process.

4.2 Estimates of the diffusion coefficient of Nd in liquid Magnesium, D

Values for the parameters (Cs, Cz, C_i and δ) in Equation 1 and 2 can be determined by observation of Figure 16. The values of these parameters are shown in the Table 12. Note that the adjusted Nd composition values which take the contribution of Pr, Dy and B into

Table 12. Parameters in Equation 1 and 2 determined by Figure 16.

	Nd composition			Thickness of boundary layer
	Cs (wt.%)	Cz (wt.%)	C_i (wt.%)	δ (μm)
Measured values	27.36	1.02	12.18	74.0
Adjusted values	18.0	0.67	8.01	___

account are based on the scrap having an initial Nd composition around 18.0wt.%. These values can be used to obtain an estimate of the temperature dependent diffusion coefficient for Nd in liquid Mg derived from the Equation 1, 2 and 3:

$$D \approx (C_s - C_z)\frac{dL}{dt}\frac{\delta}{C_i} \qquad (4)$$

Substituting the values in Table 12 into Equation 4 gives $D_{725}=4.38\times10^{-8}cm^2/sec$. The same method can be used to solve for the diffusion coefficient at the other temperatures. For the other calculations, it was assumed that Cs, Cz, C_i and δ remained relatively constant. This assumption is believed to be fairly accurate for the following reasons. Firstly, the convection currents in the molten Mg which determine C_i and δ are expected to be sufficiently rapid for all the experimental conditions used to cause similar values for C_i and δ. Secondly, the

contrast of the diffusion layers using BSE for all the samples was essentially identical, indicating that Cz is fairly constant. Thus, only the changes in T, t and L need be considered to calculate the diffusion coefficient. Following the same procedure as for the 725°C data, the calculated diffusion coefficients for the other temperatures are listed in Table 13. Note that the calculated diffusion coefficients are the same no matter whether the measured Nd composition or the adjusted Nd composition is used. This is because the Nd composition used in Equation 4 is based on the relative changes in composition rather than absolute values. As expected, the diffusion coefficient increases from 675°C to 750°C.

It is known the diffusion coefficient is a function of temperature, and can be represented by an Arrhenius relationship of the form [23]:

$$D = D_0 e^{-Q/RT} \qquad (5)$$

Table 13. Calculated values of diffusion coefficient of Nd in liquid Mg, D.

Casting Temperature	Calculated average Diffusion Coefficient D (cm^2/sec)
675°C	4.20×10^{-10}
700°C	4.61×10^{-8}
725°C	4.78×10^{-8}
750°C	8.98×10^{-8}

An estimate of the temperature independent constant D_0 and the activation energy Q can be made by plotting lnD versus 1/T which gives D_0 as the y-intercept and –Q/R as the slope. Since only one data point was obtained at 675°C, that point was omitted from subsequent analysis. This is shown in Figure 18. Obtaining a best fitted line to the 700°C, 725°C, and 750°C data allows the values for D_0 and Q to be calculated using standard methods. Doing this gives D_0 and Q are $2.16\times10^{-2}cm^2/sec$ and $1.06\times10^2KJ/mol$, respectively.

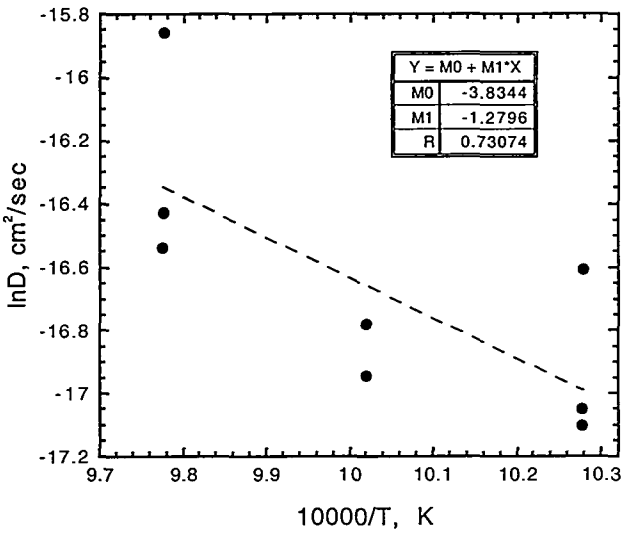

Figure 18. The plot of lnD versus 1/T.

These calculated D_0 and Q values refer to the rate of diffusion for Nd in liquid Mg. Although no other data could be found concerning rare earths diffusion in molten Mg, data does exist on the diffusion of Ce and La through solid Mg [26]. Table 14 compares the D_0 and Q values determined experimentally in this study to the existing data for rare earths in solid Mg. Note that the D_0 values for Ce and La in solid Mg varies widely, on the scale of

four orders of magnitude. This is surprising since the metallic radii (Å) and atomic volumes (cm^3/mol) of Ce and La atoms are relatively close, being 1.82 : 1.88 and 20.70 : 22.60 respectively. Equally surprising is that the D_0 and Q for Nd in liquid Mg are very close to the values for La in solid Mg. Clearly, further work needs to be done on the diffusion of rare earths in solid and liquid Mg before any definite conclusions can be drawn.

Table 14. The calculated D_0 and Q for diffusion rate for Nd in liquid Mg as compared to diffusion rate of Mg and rare earth (Ce and La) in solid Mg.

	Mg in Solid Mg	Ce in Solid Mg	La in Solid Mg	Nd in Liquid Mg
D_0 (cm^2/sec)	1.5	4.50×10^{2}	2.20×10^{-2}	2.16×10^{-2}
Q (KJ/mol)	1.36×10^{2}	1.76×10^{2}	1.02×10^{2}	1.06×10^{2}
Temperature Range (°C)	467 — 635	500 — 600	500 — 600	700 — 750

5 SUMMARY AND CONCLUSIONS

1. Using molten magnesium to remove Nd from NdFeB magnet scrap and particulate with size range from 20mesh to 50mesh by diffusion is an effective method of recovering Nd from waste by-products of rare earth magnet manufacture. Diffusion proceeds rapidly at temperatures above 700°C, enriching the Mg with Nd.
2. The molten Mg matrix consists of two phases upon solidification: a binary eutectic consisting of solid solution α-Mg + Nd and $Mg_{12}Nd$. The $Mg_{12}Nd$ is present in two forms, intergranularly and as Widmanstatten plates within the grains.
3. From the Nd composition profile across the diffusion layer, a two-phase zone forms which contains very little Nd. If one assumes that the average composition of Nd in the two-phase zone remains constant at Cz, and the thickness of the boundary layer in liquid Mg at the solid / liquid interface δ remains constant during the casting process, the mass transport process of Nd through NdFeB scrap can be explained.
4. By letting the flux of Nd out of the scrap equal the flux into the liquid Mg, the diffusion coefficient of Nd in liquid Mg can be calculated. Doing this gives diffusion coefficients of Nd in liquid Mg larger than 4.61×10^{-8} cm^2/sec at temperatures above 700°C.

APPENDIX

Table 15. The composition data collected by EDS line scan from the sample cast at 725°C for 8 hours across the diffusion layer, the composition profile is shown in Figure 15.

Step	Mg (wt.%)	Fe (wt.%)	Nd (wt.%)	Step	Mg (wt.%)	Fe (wt.%)	Nd (wt.%)
1.0000	1.7500	72.790	25.460	45.000	1.8000	72.200	26.000
2.0000	1.9700	73.630	24.400	46.000	2.1300	71.380	26.490
3.0000	2.0200	73.310	24.660	47.000	1.4200	72.600	25.980
4.0000	1.4600	71.850	26.680	48.000	1.6100	72.560	25.830
5.0000	2.4400	59.940	37.610	49.000	1.5300	71.850	26.620
6.0000	2.4100	60.850	36.740	50.000	1.6600	70.980	27.360
7.0000	1.7400	72.300	25.960	51.000	2.0500	71.870	26.080
8.0000	1.7600	71.830	26.410	52.000	2.0300	71.900	26.070
9.0000	1.6000	71.760	26.630	53.000	1.4800	71.740	26.780
10.000	1.5900	72.290	26.130	54.000	1.5300	71.980	26.490
11.000	1.5500	71.490	26.950	55.000	1.6700	72.400	25.930
12.000	1.6900	71.020	27.290	56.000	1.6500	71.750	26.600
13.000	1.7700	70.920	27.310	57.000	1.7600	71.890	26.340
14.000	2.0800	73.020	24.910	58.000	4.5700	86.160	9.2700
15.000	2.6300	71.010	26.360	59.000	4.3500	85.380	10.270
16.000	2.5900	70.490	26.920	60.000	1.0200	98.290	0.6900
17.000	2.0400	73.420	24.540	61.000	1.3900	97.120	1.4900
18.000	2.2800	74.290	23.430	62.000	1.6600	96.970	1.3700
19.000	1.8700	71.180	26.950	63.000	0.8100	99.160	0.0200
20.000	2.2600	71.340	26.400	64.000	1.1000	98.840	0.0500
21.000	2.2500	71.630	26.110	65.000	1.0200	98.660	0.3200
22.000	1.8600	72.510	25.630	66.000	4.2900	94.690	1.0200
23.000	1.9400	71.690	26.370	67.000	4.1300	94.630	1.2400
24.000	2.0600	71.090	26.850	68.000	1.3500	97.730	0.9100
25.000	4.4200	68.250	27.330	69.000	3.5900	94.930	1.4800
26.000	4.8100	66.750	28.440	70.000	3.7700	95.250	0.9800
27.000	1.2400	97.930	0.8200	71.000	1.2600	97.990	0.7500
28.000	1.9200	72.440	25.630	72.000	1.5100	97.670	0.8200
29.000	1.8700	71.720	26.410	73.000	2.3700	94.570	3.0600
30.000	3.4800	70.020	26.490	74.000	1.7900	71.890	26.320
31.000	1.7700	71.830	26.400	75.000	1.7700	72.630	25.600
32.000	2.0600	89.760	8.1700	76.000	1.6100	72.250	26.130
33.000	2.0100	71.150	26.840	77.000	1.4200	78.930	19.650
34.000	1.9500	71.590	26.460	78.000	1.3800	80.210	18.410
35.000	1.7000	72.610	25.700	79.000	1.4200	98.170	0.4100
36.000	1.6300	70.810	27.560	80.000	1.3200	97.870	0.8100
37.000	1.5800	71.690	26.730	81.000	1.7500	95.890	2.3600
38.000	2.7600	71.070	26.170	82.000	1.8700	95.260	2.8700
39.000	2.8600	71.420	25.720	83.000	2.3100	82.170	15.520
40.000	1.6700	72.150	26.180	84.000	1.7700	88.700	9.5300
41.000	1.6000	72.110	26.290	85.000	1.7400	88.750	9.5100
42.000	1.7500	71.390	26.860	86.000	1.7100	72.670	25.620
43.000	1.5900	71.370	27.040	87.000	6.0000	89.880	4.1200
44.000	1.7500	71.670	26.590	88.000	6.2100	89.520	4.2700

Table 15. (continued)

89.000	1.9200	97.630	0.4500	147.00	3.1900	94.740	2.0700
90.000	1.8500	97.450	0.7000	148.00	3.9900	68.500	27.510
91.000	1.0900	98.690	0.2100	149.00	3.6200	87.950	8.4400
92.000	1.8500	96.590	1.5500	150.00	3.4500	87.810	8.7400
93.000	1.5500	97.570	0.8800	151.00	2.8800	95.930	1.1900
94.000	1.4200	95.700	2.8800	152.00	3.0500	96.070	0.8800
95.000	1.4900	96.400	2.1100	153.00	0.5600	99.200	0.2400
96.000	1.3200	98.280	0.4000	154.00	6.7700	92.450	0.7800
97.000	2.3800	97.550	0.0600	155.00	6.6300	92.360	1.0100
98.000	2.6900	96.490	0.8200	156.00	4.1800	88.140	7.6900
99.000	3.8700	94.650	1.4800	157.00	3.9400	87.400	8.6600
100.00	1.1900	98.340	0.4700	158.00	1.2400	97.680	1.0800
101.00	1.2000	98.200	0.6000	159.00	4.0500	90.710	5.2400
102.00	3.0800	95.490	1.4300	160.00	4.0000	90.400	5.6000
103.00	3.0300	95.000	1.9700	161.00	2.1900	96.590	1.2200
104.00	3.0900	75.910	21.000	162.00	1.2400	98.380	0.3800
105.00	2.1900	96.560	1.2600	163.00	1.5500	97.670	0.7800
106.00	2.3400	96.460	1.2100	164.00	1.1700	98.270	0.5500
107.00	3.9800	91.450	4.5600	165.00	1.1400	98.680	0.1800
108.00	4.2400	91.320	4.4500	166.00	1.1100	98.590	0.3000
109.00	1.6000	97.730	0.6700	167.00	1.1600	98.190	0.6600
110.00	1.9500	96.670	1.3800	168.00	1.2300	98.040	0.7300
111.00	1.9800	97.310	0.7100	169.00	1.0500	99.050	-0.100
112.00	1.6900	97.550	0.7500	170.00	1.3400	98.050	0.6000
113.00	4.1300	92.180	3.6900	171.00	4.8200	91.780	3.4000
114.00	3.7900	92.710	3.4900	172.00	32.720	51.630	15.660
115.00	4.9500	91.100	3.9500	173.00	33.060	52.440	14.490
116.00	5.0000	90.920	4.0800	174.00	16.810	71.150	12.050
117.00	3.2700	95.260	1.4800	175.00	16.720	72.620	10.660
118.00	3.1100	95.010	1.8800	176.00	1.0900	98.320	0.5900
119.00	2.6400	95.480	1.8800	177.00	2.1000	96.760	1.1500
120.00	2.1600	94.430	3.4000	178.00	2.0400	96.980	0.9800
121.00	2.3100	94.040	3.6400	179.00	4.6300	92.430	2.9400
122.00	1.9600	94.420	3.6200	180.00	4.3300	93.140	2.5300
123.00	1.3500	97.500	1.1500	181.00	2.9800	94.770	2.2500
124.00	1.6000	98.080	0.3200	182.00	3.0000	65.950	31.040
125.00	6.9600	89.880	3.1500	183.00	2.9100	66.440	30.650
126.00	1.7500	97.540	0.7100	184.00	6.7200	86.430	6.8400
127.00	1.6600	97.740	0.6100	185.00	2.4900	95.780	1.7300
128.00	0.9900	98.810	0.1900	186.00	2.3900	95.800	1.8200
129.00	1.0400	98.480	0.4800	187.00	2.5700	95.130	2.3000
130.00	7.9200	86.750	5.3300	188.00	2.6200	95.400	1.9800
131.00	8.2500	86.690	5.0600	189.00	1.9400	97.250	0.8100
132.00	1.0600	98.670	0.2700	190.00	2.1600	95.980	1.8600
133.00	1.3100	98.290	0.4100	191.00	2.0800	96.810	1.1100
134.00	1.4700	98.400	0.1300	192.00	1.8300	97.260	0.9200
135.00	2.9400	95.060	2.0000	193.00	1.8900	97.160	0.9600
136.00	1.4700	98.450	0.0900	194.00	4.6100	89.510	5.8700
137.00	1.4800	98.400	0.1200	195.00	2.5300	95.310	2.1700
138.00	10.480	84.570	4.9600	196.00	2.6100	94.650	2.7400
139.00	10.110	84.110	5.7800	197.00	2.6500	94.040	3.3100
140.00	16.760	79.580	3.6500	198.00	1.4100	97.700	0.8800
141.00	1.5600	97.830	0.6200	199.00	1.5500	97.160	1.2900
142.00	1.7400	97.300	0.9600	200.00	1.3200	98.130	0.5500
143.00	1.3000	97.360	1.3400	201.00	1.5300	97.770	0.7000
144.00	1.4200	98.240	0.3400	202.00	2.1300	94.020	3.8500
145.00	1.2000	98.410	0.3900	203.00	2.0800	93.840	4.0800
146.00	3.1000	95.800	1.0900	204.00	1.5700	97.920	0.5200

Table 15. (continued)

205.00	1.6300	97.560	0.8100	263.00	2.9200	91.170	5.9100
206.00	1.7700	96.800	1.4300	264.00	9.3300	72.900	17.770
207.00	2.5900	96.130	1.2800	265.00	8.7000	73.910	17.380
208.00	1.0400	98.680	0.2800	266.00	5.7900	92.080	2.1300
209.00	1.1300	98.650	0.2200	267.00	2.2200	98.210	-0.440
210.00	2.6400	86.300	11.060	268.00	2.0900	97.370	0.5400
211.00	2.8200	85.150	12.030	269.00	1.9500	97.430	0.6200
212.00	1.8700	97.530	0.6000	270.00	4.0000	92.600	3.4000
213.00	5.1200	87.240	7.6400	271.00	3.7700	92.640	3.5900
214.00	4.9500	87.660	7.4000	272.00	3.6900	94.900	1.4100
215.00	2.8100	64.600	32.590	273.00	3.8200	94.770	1.4000
216.00	2.6800	63.790	33.520	274.00	1.9500	96.670	1.3700
217.00	1.7500	95.950	2.3100	275.00	1.9600	97.400	0.6500
218.00	8.7500	82.260	9.0000	276.00	1.8800	97.310	0.8100
219.00	9.2400	82.840	7.9200	277.00	1.8500	97.950	0.2000
220.00	2.6600	95.040	2.3000	278.00	1.7500	97.940	0.3100
221.00	0.8400	98.770	0.3900	279.00	11.050	84.960	3.9900
222.00	1.0400	98.740	0.2200	280.00	2.6100	95.430	1.9700
223.00	1.7900	96.970	1.2400	281.00	2.7000	95.680	1.6100
224.00	1.8400	96.710	1.4500	282.00	2.5300	96.670	0.8100
225.00	1.6800	96.210	2.1100	283.00	2.1500	97.240	0.6100
226.00	1.0300	98.170	0.8000	284.00	2.2200	97.390	0.4000
227.00	1.0300	98.800	0.1800	285.00	4.7800	93.440	1.7800
228.00	2.6500	96.700	0.6500	286.00	4.8400	93.460	1.7000
229.00	2.4500	96.730	0.8200	287.00	2.1600	97.620	0.2200
230.00	2.9900	96.480	0.5300	288.00	2.0700	97.230	0.7000
231.00	1.0500	99.030	-0.070	289.00	2.0300	97.550	0.4200
232.00	0.8800	99.230	-0.120	290.00	2.4600	96.760	0.7800
233.00	5.6700	91.020	3.3100	291.00	2.3200	96.840	0.8400
234.00	3.7100	94.350	1.9400	292.00	1.7600	97.650	0.5900
235.00	3.5500	94.360	2.0900	293.00	7.7100	87.300	4.9900
236.00	2.3500	96.370	1.2800	294.00	8.0700	86.840	5.0900
237.00	2.1000	96.360	1.5400	295.00	2.1400	95.640	2.2100
238.00	1.5900	97.930	0.4900	296.00	1.9200	96.130	1.9500
239.00	1.6200	98.140	0.2400	297.00	1.5200	98.060	0.4200
240.00	1.7800	97.350	0.8700	298.00	2.5200	97.070	0.4000
241.00	2.0000	96.830	1.1700	299.00	2.4200	96.640	0.9400
242.00	1.7300	96.430	1.8400	300.00	8.7300	90.010	1.2600
243.00	12.230	78.140	9.6300	301.00	8.4000	89.570	2.0300
244.00	4.5200	92.910	2.5700	302.00	6.0800	93.490	0.4300
245.00	4.4600	92.820	2.7300	303.00	2.9700	96.140	0.8900
246.00	1.4900	97.240	1.2700	304.00	3.0200	95.680	1.3000
247.00	3.0400	95.900	1.0600	305.00	2.7700	97.040	0.1900
248.00	3.1000	95.190	1.7000	306.00	3.8200	95.230	0.9500
249.00	1.2200	98.290	0.4900	307.00	3.9500	95.300	0.7400
250.00	1.2400	98.190	0.5700	308.00	6.1300	92.610	1.2600
251.00	4.8100	92.150	3.0400	309.00	6.0500	93.620	0.3300
252.00	4.8700	92.610	2.5200	310.00	4.0100	97.000	-1.020
253.00	2.1600	96.760	1.0800	311.00	9.4600	84.980	5.5600
254.00	1.7700	98.050	0.1700	312.00	9.5900	85.430	4.9800
255.00	1.9500	98.130	-0.080	313.00	2.6300	97.980	-0.6100
256.00	1.6300	96.820	1.5500	314.00	2.6200	98.600	-1.2200
257.00	5.2600	90.570	4.1700	315.00	6.1400	91.540	2.32000
258.00	5.5800	90.670	3.7500	316.00	3.7700	97.370	-1.1400
259.00	2.3500	95.950	1.7000	317.00	3.7400	97.020	-0.7600
260.00	2.5500	96.180	1.2600	318.00	2.7500	99.210	-1.9500
261.00	1.6900	97.890	0.4100	319.00	50.330	63.610	-13.930
262.00	3.0100	91.800	5.2000	320.00	48.160	63.180	-11.330

Table 15. (continued)

321.00	3.5300	98.250	-1.7800	361.00	95.540	0.22000	4.2400
322.00	3.5300	97.830	-1.3600	362.00	96.550	0.11000	3.3300
323.00	89.560	1.9100	8.5300	363.00	96.590	0.13000	3.2800
324.00	89.670	2.6100	7.7300	364.00	95.820	0.28000	3.9000
325.00	87.230	1.0300	11.740	365.00	96.460	-0.0300	3.5800
326.00	87.080	2.5400	10.380	366.00	97.060	-0.2100	3.1500
327.00	87.720	1.6300	10.660	367.00	97.040	0.12000	2.8400
328.00	87.870	1.3000	10.830	368.00	62.400	0.44000	37.160
329.00	88.340	1.7700	9.8900	369.00	62.080	0.09000	37.830
330.00	89.910	1.1800	8.9100	370.00	62.910	-0.2200	37.310
331.00	90.180	1.3900	8.4300	371.00	62.540	0.28000	37.180
332.00	89.290	1.9000	8.8100	372.00	62.470	-0.0700	37.600
333.00	93.950	0.2700	5.7700	373.00	62.140	-0.0400	37.900
334.00	94.210	0.4600	5.3300	374.00	62.760	-0.1100	37.360
335.00	93.750	0.2600	5.9900	375.00	61.930	0.26000	37.810
336.00	94.060	0.3300	5.6100	376.00	62.430	0.12000	37.450
337.00	94.330	0.2400	5.4300	377.00	86.190	0.09000	13.720
338.00	93.250	0.3500	6.4000	378.00	97.800	0.18000	2.0100
339.00	95.250	0.1600	4.6000	379.00	97.480	0.47000	2.0400
340.00	94.910	0.2900	4.8000	380.00	97.160	0.25000	2.5800
341.00	94.610	0.1200	5.2700	381.00	97.400	0.07000	2.5300
342.00	96.040	0.2000	3.7700	382.00	96.560	0.13000	3.3100
343.00	96.020	0.0300	3.9500	383.00	97.070	0.24000	2.6900
344.00	94.070	0.2900	5.6400	384.00	97.050	0.26000	2.6900
345.00	93.500	0.3300	6.1700	385.00	96.610	0.15000	3.2400
346.00	82.500	-0.220	17.720	386.00	96.660	-0.1000	3.4400
347.00	73.740	0.7100	25.550	387.00	96.620	0.36000	3.0200
348.00	75.530	0.0100	24.450	388.00	97.200	0.10000	2.7000
349.00	94.480	0.2400	5.2900	389.00	96.920	0.09000	2.9900
350.00	93.980	0.2400	5.7800	390.00	97.300	0.38000	2.3200
351.00	96.410	-0.030	3.6200	391.00	97.450	0.21000	2.3500
352.00	97.500	0.17000	2.3300	392.00	96.980	0.36000	2.6700
353.00	97.330	0.27000	2.4000	393.00	97.160	0.18000	2.6500
354.00	96.700	0.26000	3.0400	394.00	97.170	0.16000	2.6600
355.00	96.370	0.22000	3.4100	395.00	96.940	0.39000	2.6600
356.00	96.160	0.45000	3.3900	396.00	97.180	0.30000	2.5200
357.00	95.540	0.20000	4.2600	397.00	97.320	0.30000	2.3900
358.00	96.420	-0.1100	3.6900	398.00	97.340	0.28000	2.3800
359.00	97.020	0.10000	2.8800	399.00	97.410	0.11000	2.4700
360.00	96.250	0.23000	3.5200	400.00	97.490	0.14000	2.3600

REFERENCES

1. J. G. Cannon, *Engineering and Mining Journal*, March 1983, pp. 136-137.
2. M. Sagawa, S. Fujimura, N. Togawa, H. Yamamoto, and Y. Matsuura, *Journal of Applied Physics*, vol. 55(6), 1984, pp. 2083-2087.
3. J. Robbins, *Materials Edge*, Sept./Oct. 1988, pp. 51-52.
4. M. Honshima, and K. Ohashi, *Journal of Materials Engineering and Performance*, vol. 3(2), April 1994, pp. 218-222.
5. J. W. Fiepke, *Hard and Soft Magnetic Materials with Applications Including Superconductivity*, ASM International, Metals Park, Ohio 44073, 1987, pp. 75-80.
6. J. D. Livingston, *Journal of Metals*, Feb. 1990, pp. 30-34.
7. J. W. Morrison, and G. R. Palmer, *Recycling of Metals and Engineered Materials*, TMS, Warrendale, PA, 1990, pp. 593-609.
8. J. W. Lyman, and G. R. Palmer, *High Temperature Materials and Processes*, vol. 11(1-4), Jan. 1993, pp. 175-187.
9. B. Greenberg, *Neodymium Recovery Process*, U. S. Patent 5,362,459, Nov. 8, 1994.
10. F. A. Schmidt, and D. T. Peterson, *Method for Treating Rare Earth-transition Metal Scrap*, U. S. Patent 5,174,811, Dec. 29, 1992.
11. F. A. Schmidt, and D. T. Peterson, *Rare Earth-transition Metal Scrap Treatment Method*, U. S. Patent 5,087,291, Feb. 11, 1992.
12. D. T. Peterson, and R. Kontrimas, *Journal of Physical Chemistry*, vol. 64, 1960, pp. 362.
13. T. W. Ellis, F. A. Schmidt, and L. L. Jones, *Metals and Materials Waste Reduction, Recovery and Remediation*, TMS, Warrendale, PA, 1994, pp. 199-206.

14. A. P. Bayanov, S. F. Gurskaya, and V. V. Serebrennikov, *Zhurnal Prikladnoi Khimii*, vol.39(2), 1966, pp. 447-448.

15. R. Kontrimas, *Distribution of Metals between Liquid Lead and Liquid Zinc*, Iowa State University, Ames, IA, Ph.D. Dissertation, 1961.

16. T. W. Ellis, and F. A. Schmidt, *Recycling of Rare Earth Metals from Rare Earth-transition Metal Alloy Scrap by Liquid Metal Extraction*, U. S. Patent 5,437,709, Aug. 1, 1995.

17. T. B. Massalski, J. L. Murray, L. H. Bennett, and H. Baker, *Binary Alloy Phase Diagrams*, ASM, Metals Park, Ohio 44073, vol. 1, 1986, pp. 1077 and pp. 1527.

18. I. Yu. Mukhina, V. M. Lebedev, Kyung-Hyun Kim, and In-Bae Kim, *Journal of Advanced Materials*, vol. 3(5), 1996, pp. 362-369.

19. Discussion with Ken Clark, then at Fansteel - Wellman Dynamics, of Creston, IA.

20. W. Zhang, G. Liu, and K. Han, *Journal of Phase Equilibria*, vol. 13(6), 1992.

21. Joachim Wecker, *Zeitschrift fur Metallkunde*, vol. 81(3), 1990, pp. 157-165.

22. P. Villars, A. Prince, and H. Okamoto, *Handbook of Ternary Alloy Phase Diagrams*, ASM, Materials Park, OH, vol. 5, 1995, pp. 5599-5619.

23. J. D. Verhoeven, *Fundamentals of Physical Metallurgy*, Wiley & Sons, New York, NY, 1975, pp. 145.

24. P. G. Shewmon, *Diffusion in Solids*, TMS, Warrendale, PA, 1989, pp. 131-148.

25. G. H. Geiger, and D. R. Poirier, *Transport Phenomena in Metallurgy*, Addison-Wesley, 1980, pp. 431.

26. Krishan Lal, and Viviane Levy, *Comptes Rendus Acad. Sc. Paris*, vol. 262, Jan. 1966, pp. 107-109.

ACKNOWLEDGEMENTS

This work was partially funded by a Carver Trust grant from Iowa State University and was performed at Ames Laboratory under Contract No. W-7405-Eng82 with the U. S. Department of Energy. The United States government has assigned the DOE Report number IS-T 1872 to this thesis.

I would like to thank the Program of Study Committee who helped plan and direct this project: Profs. Scott Chumbley (chair), Alan Russell and Frank Peters. I am deeply grateful to my major professor, Dr. Scott Chumbley, for his support, guidance, patience and encouragement.

Special thanks go to L. Lincoln, C. Gross and F. Laabs of the Ames Laboratory Materials Preparation Center for preparing and analyzing the materials used in this study. The guidance of F. Schmidt and T.W. Ellis is especially appreciated.

Also, I thank all of my officemates, Zhan Shi, Vladimir Gantovnik and Kai Xu, and my whole family for their helpful suggestion and support through my studies.